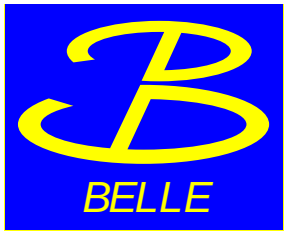


BELLE Preprint 2008-16
KEK Preprint 2008-10



# High-Statistics Study of the $\tau^- \to \pi^- \pi^0 \nu_\tau$ Decay

M. Fujikawa,[23] H. Hayashii,[23] S. Eidelman,[1] I. Adachi,[7] H. Aihara,[42] K. Arinstein,[1] V. Aulchenko,[1] T. Aushev,[18,13] A. M. Bakich,[40] V. Balagura,[13] E. Barberio,[21] A. Bay,[18] I. Bedny,[1] K. Belous,[12] V. Bhardwaj,[33] U. Bitenc,[14] A. Bondar,[1] M. Bračko,[20,14] J. Brodzicka,[7] T. E. Browder,[6] P. Chang,[26] Y. Chao,[26] A. Chen,[24] B. G. Cheon,[5] R. Chistov,[13] I.-S. Cho,[47] Y. Choi,[39] J. Dalseno,[7] M. Dash,[46] D. Epifanov,[1] N. Gabyshev,[1] B. Golob,[19,14] H. Ha,[16] J. Haba,[7] K. Hara,[22] Y. Hasegawa,[38] K. Hayasaka,[22] M. Hazumi,[7] D. Heffernan,[32] Y. Hoshi,[41] W.-S. Hou,[26] H. J. Hyun,[17] T. Iijima,[22] K. Inami,[22] A. Ishikawa,[35] H. Ishino,[43] R. Itoh,[7] M. Iwabuchi,[4] M. Iwasaki,[42] D. H. Kah,[17] H. Kaji,[22] S. U. Kataoka,[23] T. Kawasaki,[29] H. Kichimi,[7] H. O. Kim,[17] S. K. Kim,[37] Y. I. Kim,[17] Y. J. Kim,[4] S. Korpar,[20,14] P. Križan,[19,14] P. Krokovny,[7] R. Kumar,[33] A. Kuzmin,[1] Y.-J. Kwon,[47] S.-H. Kyeong,[47] J. S. Lange,[3] M. J. Lee,[37] S. E. Lee,[37] A. Limosani,[21] C. Liu,[36] Y. Liu,[4] D. Liventsev,[13] J. MacNaughton,[7] F. Mandl,[11] A. Matyja,[27] S. McOnie,[40] K. Miyabayashi,[23] H. Miyata,[29] Y. Miyazaki,[22] R. Mizuk,[13] G. R. Moloney,[21] T. Mori,[22] Y. Nagasaka,[8] E. Nakano,[31] M. Nakao,[7] H. Nakazawa,[24] Z. Natkaniec,[27] S. Nishida,[7] O. Nitoh,[45] S. Noguchi,[23] T. Nozaki,[7] T. Ohshima,[22] S. Okuno,[15] S. L. Olsen,[6,10] H. Ozaki,[7] P. Pakhlov,[13] G. Pakhlova,[13] H. Palka,[27] C. W. Park,[39] H. Park,[17] H. K. Park,[17] L. S. Peak,[40] R. Pestotnik,[14] L. E. Piilonen,[46] A. Poluektov,[1] H. Sahoo,[6] Y. Sakai,[7] O. Schneider,[18] A. J. Schwartz,[2] R. Seidl,[9,34] A. Sekiya,[23] K. Senyo,[22] M. E. Sevior,[21] M. Shapkin,[12] V. Shebalin,[1] C. P. Shen,[10] J.-G. Shiu,[26] B. Shwartz,[1] J. B. Singh,[33] A. Sokolov,[12] S. Stanič,[30] M. Starič,[14] T. Sumiyoshi,[44] F. Takasaki,[7] N. Tamura,[29] M. Tanaka,[7] G. N. Taylor,[21] Y. Teramoto,[31] K. Trabelsi,[7] T. Tsuboyama,[7] S. Uehara,[7] T. Uglov,[13] Y. Unno,[5] S. Uno,[7] P. Urquijo,[21] Y. Usov,[1] G. Varner,[6] K. Vervink,[18] A. Vinokurova,[1] C. H. Wang,[25] P. Wang,[10] X. L. Wang,[10] Y. Watanabe,[15] E. Won,[16] Y. Yamashita,[28] M. Yamauchi,[7] C. Z. Yuan,[10] C. C. Zhang,[10] Z. P. Zhang,[36] V. Zhilich,[1] V. Zhulanov,[1] T. Zivko,[14] A. Zupanc,[14] and O. Zyukova[1]

(The Belle Collaboration)

[1] *Budker Institute of Nuclear Physics, Novosibirsk*
[2] *University of Cincinnati, Cincinnati, Ohio 45221*
[3] *Justus-Liebig-Universität Gießen, Gießen*
[4] *The Graduate University for Advanced Studies, Hayama*
[5] *Hanyang University, Seoul*
[6] *University of Hawaii, Honolulu, Hawaii 96822*
[7] *High Energy Accelerator Research Organization (KEK), Tsukuba*
[8] *Hiroshima Institute of Technology, Hiroshima*
[9] *University of Illinois at Urbana-Champaign, Urbana, Illinois 61801*

[10]*Institute of High Energy Physics, Chinese Academy of Sciences, Beijing*
[11]*Institute of High Energy Physics, Vienna*
[12]*Institute of High Energy Physics, Protvino*
[13]*Institute for Theoretical and Experimental Physics, Moscow*
[14]*J. Stefan Institute, Ljubljana*
[15]*Kanagawa University, Yokohama*
[16]*Korea University, Seoul*
[17]*Kyungpook National University, Taegu*
[18]*École Polytechnique Fédérale de Lausanne (EPFL), Lausanne*
[19]*Faculty of Mathematics and Physics, University of Ljubljana, Ljubljana*
[20]*University of Maribor, Maribor*
[21]*University of Melbourne, School of Physics, Victoria 3010*
[22]*Nagoya University, Nagoya*
[23]*Nara Women's University, Nara*
[24]*National Central University, Chung-li*
[25]*National United University, Miao Li*
[26]*Department of Physics, National Taiwan University, Taipei*
[27]*H. Niewodniczanski Institute of Nuclear Physics, Krakow*
[28]*Nippon Dental University, Niigata*
[29]*Niigata University, Niigata*
[30]*University of Nova Gorica, Nova Gorica*
[31]*Osaka City University, Osaka*
[32]*Osaka University, Osaka*
[33]*Panjab University, Chandigarh*
[34]*RIKEN BNL Research Center, Upton, New York 11973*
[35]*Saga University, Saga*
[36]*University of Science and Technology of China, Hefei*
[37]*Seoul National University, Seoul*
[38]*Shinshu University, Nagano*
[39]*Sungkyunkwan University, Suwon*
[40]*University of Sydney, Sydney, New South Wales*
[41]*Tohoku Gakuin University, Tagajo*
[42]*Department of Physics, University of Tokyo, Tokyo*
[43]*Tokyo Institute of Technology, Tokyo*
[44]*Tokyo Metropolitan University, Tokyo*
[45]*Tokyo University of Agriculture and Technology, Tokyo*
[46]*Virginia Polytechnic Institute and State University, Blacksburg, Virginia 24061*
[47]*Yonsei University, Seoul*

## Abstract

We report a high-statistics measurement of the branching fraction for $\tau^- \to \pi^-\pi^0\,\nu_\tau$ and the invariant mass spectrum of the produced $\pi^-\pi^0$ system using 72.2 fb$^{-1}$ of data recorded with the Belle detector at the KEKB asymmetric-energy $e^+e^-$ collider. The branching fraction obtained is $(25.24 \pm 0.01 \pm 0.39)\%$, where the first error is statistical and the second is systematic. The unfolded $\pi^-\pi^0$ mass spectrum is used to determine resonance parameters for the $\rho(770)$, $\rho'(1450)$, and $\rho''(1700)$ mesons. We also use this spectrum to estimate the hadronic $(2\pi)$ contribution to the anomalous magnetic moment of the muon $(a_\mu^{\pi\pi})$. Our result for $a_\mu^{\pi\pi}$ integrated over the mass range $\sqrt{s} = 2m_\pi - 1.8$ GeV/$c^2$ is $a_\mu^{\pi\pi} = (523.5 \pm 1.5\,(\mathrm{exp}) \pm 2.6\,(\mathrm{Br}) \pm 2.5\,(\mathrm{isospin})) \times 10^{-10}$, where the first error is due to the experimental uncertainties, the second is due to the uncertainties in the branching fractions and the third is due to the uncertainties in the isospin-violating corrections.



PACS numbers: 13.40.Gp, 13.35.Dx, 14.60.Fg

## I. INTRODUCTION

Hadronic decays of the $\tau$ lepton provide a clean environment for studying the dynamics of hadronic states with various quantum numbers. Among the decay channels of the $\tau$ lepton, $\tau^-\to\pi^-\pi^0\,\nu_\tau$ has the largest branching fraction [1]. The decay is dominated by intermediate resonances and thus can be used to extract information on the properties of the $\rho(770)$, $\rho'(1450)$, and $\rho''(1700)$ mesons and their mutual interference.

From the conservation of vector current (CVC) theorem, the $\pi^-\pi^0$ mass spectrum in this range can be related to the cross section for the process $e^+e^-\to\pi^+\pi^-$ and thus used to improve the theoretical error on the anomalous magnetic moment of the muon $a_\mu=(g_\mu-2)/2$. Recent reviews of calculations of $a_\mu$ are given in Refs. [2, 3, 4]. It is known that the theoretical error on $a_\mu$ is dominated by the contribution from the leading-order hadronic vacuum polarization $a_\mu^{\rm had,LO}$. This contribution cannot be derived within the framework of perturbative QCD and is usually evaluated using dispersion relations and the experimental cross section for $e^+e^-$ annihilation to hadrons [5, 6, 7, 8]. Alternatively, CVC relates the properties of the $\pi^+\pi^-$ system produced in $e^+e^-\to\pi^+\pi^-$ to those of the $\pi^-\pi^0$ system produced in $\tau^-\to\pi^-\pi^0\,\nu_\tau$ decay; thus, using CVC and correcting for isospin-violating effects, $\tau$ data have also been used to obtain a more precise prediction for $a_\mu^{\rm had,LO}$ [5, 6, 8, 9].

Recently, new precise data on $e^+e^-\to\pi^+\pi^-$ have become available from the CMD-2, KLOE, and SND experiments [10, 11, 12, 13, 14, 15, 16, 17]. ALEPH [18, 19], CLEO [20, 21], and OPAL [22, 23] measured both the $2\pi$ spectral function and the branching fraction for the $\tau^-\to\pi^-\pi^0\,\nu_\tau$ decay; the latter was also determined by L3 [24] and DELPHI [25]. Recent evaluations of the hadronic contribution to $a_\mu$ using $e^+e^-$ data result in $a_\mu^{\rm exp}-a_\mu^{\rm th}=(27.5\pm8.4)\times10^{-10}$ [26, 27], while that using the $\tau$ lepton data where applicable gives $a_\mu^{\rm exp}-a_\mu^{\rm th}=(9.4\pm10.5)\times10^{-10}$ [5], where the experimental value $a_\mu^{\rm exp}$ is dominated by the BNL E821 measurement [28] $(11\,659\,208.0\pm6.3)\times10^{-10}$. These differences correspond to 3.3 and 0.9 standard deviations, respectively. For the evaluation based on the $e^+e^-$ data, a deviation of similar size that corresponds to a $3.4\,\sigma$ discrepancy is claimed in Ref. [29]. To clarify these differences between the $e^+e^-$-based and $\tau$-based predictions, more data on $e^+e^-\to\pi^-\pi^+$ and $\tau^-\to\pi^-\pi^0\nu_\tau$ decays are needed. In this paper we present a high-statistics measurement of the $\pi^-\pi^0$ mass spectrum produced in $\tau^-\to\pi^-\pi^0\,\nu_\tau$ decays using data collected with the Belle experiment at the KEKB asymmetric-energy $e^+e^-$ collider operating at a center-of-mass (CM) energy of 10.6 GeV. The data sample is about 50 times larger than those of previous experiments.

## II. BASIC FORMULAS

The differential decay rate for $\tau^-\to\pi^-\pi^0\,\nu_\tau$ can be expressed as [30]

$$\frac{{\rm d}\Gamma(\tau^-\to\pi^-\pi^0\,\nu_\tau)}{{\rm d}s}=\Gamma_e^0\cdot\frac{6\pi|V_{ud}|^2S_{\rm EW}^{\pi\pi}}{m_\tau^2}\left(1-\frac{s}{m_\tau^2}\right)^2\left(1+\frac{2s}{m_\tau^2}\right)v_-(s),\qquad(1)$$

with

$$\Gamma_e^0=\frac{G_F^2m_\tau^5}{192\pi^3}.\qquad(2)$$

Here $s$ is the invariant mass squared of the $\pi^-\pi^0$ system, $v_-(s)$ is the weak spectral function characterizing the $\pi^-\pi^0$ system, $G_F$ is the Fermi coupling constant, $|V_{ud}|=$

$0.97377 \pm 0.00027$ [31] is the Cabibbo-Kobayashi-Maskawa (CKM) matrix element [32], $m_\tau = 1776.99^{+0.29}_{-0.26}$ MeV/$c^2$ [31] is the $\tau$ lepton mass and $S^{\pi\pi}_{\rm EW}$ accounts for short-distance electroweak radiative corrections for the $\pi^-\pi^0$ system. The measured electron decay rate of the $\tau$ lepton is related to $\Gamma^0_e$ by

$$\Gamma(\tau^- \to e^-\bar{\nu}_e\nu_\tau) \equiv \Gamma^0_e S^e_{\rm EW} = \Gamma^0_e \left\{1 + \frac{\alpha(m_\tau)}{2\pi}\left(\frac{25}{4} - \pi^2\right)\right\}, \tag{3}$$

where $S^e_{\rm EW}$ is the electroweak radiative correction for the decay $\tau^- \to e^-\bar{\nu}_e\nu_\tau$.

The corresponding $\pi^+\pi^-$spectral function $v_0(s)$ can be obtained from the $e^+e^- \to \pi^+\pi^-$ cross section

$$\sigma(e^+e^- \to \pi^+\pi^-) = \frac{4\pi^2\alpha_0^2}{s}\, v_0(s), \tag{4}$$

where $s$ is the $e^+e^-$ CM energy squared and $\alpha_0$ is the fine-structure constant at $s = 0$. Up to isospin-violating effects, CVC allows one to relate the spectral function from $\tau$ decays to the isovector part of the $e^+e^-$ spectral function [33]:

$$v_-(s) \;=\; v_0^{I=1}(s)\,. \tag{5}$$

Alternatively, the mass spectrum of the two-pion system can be expressed in terms of pion form factors, which are useful for comparing resonance shapes in the charged and neutral two-pion systems. The spectral function $v_j(s)$ $(j = -, 0)$ is related to the form factor $F^j_\pi(s)$ via

$$v_j(s) = \frac{\beta_j^3(s)}{12\pi}|F^j_\pi(s)|^2, \tag{6}$$

where $\beta_-(s)\,(\beta_0(s))$ is the pion velocity in the $\pi^-\pi^0$ $(\pi^+\pi^-)$ rest system. The velocities $\beta_j(s)$ are explicitly given by $\beta_-(s) = \lambda^{1/2}(1, m^2_{\pi^-}/s, m^2_{\pi^0}/s)$ [34] and $\beta_0(s) = \lambda^{1/2}(1, m^2_{\pi^-}/s, m^2_{\pi^-}/s) = [1 - 4m^2_{\pi^-}/s]$, with $\lambda(x, y, z) = [x - (\sqrt{y} + \sqrt{z})^2][x - (\sqrt{y} - \sqrt{z})^2]$.

The hadronic physics is contained within $v_j(s)$ or, equivalently, in $F^j_\pi(s)$. One goal of this analysis is to provide a high-precision determination of the weak form factor $|F^-_\pi(s)|$ using $\tau^- \to \pi^-\pi^0\,\nu_\tau$ data, so that a comparison with $|F^0_\pi(s)|$ from the $e^+e^-$ data can be used to test CVC. From Eqs. (1), (3) and (6), one can obtain the basic formula that expresses the form factor $F^-_\pi(s)$ in terms of the observables:

$$|F^-_\pi(s)|^2 = \frac{2m_\tau^2}{|V_{ud}|^2\left(1 - \frac{s}{m_\tau^2}\right)^2\left(1 + \frac{2s}{m_\tau^2}\right)S_{\rm EW}}\frac{1}{\beta_-^3}\left(\frac{\mathcal{B}_{\pi\pi}}{\mathcal{B}_e}\right)\left(\frac{1}{N_{\pi\pi}}\frac{{\rm d}N_{\pi\pi}}{{\rm d}s}\right), \tag{7}$$

where $\mathcal{B}_{\pi\pi}$ is the branching fraction, $(1/N_{\pi\pi})({\rm d}N_{\pi\pi}/{\rm d}s)$ is the normalized invariant mass-squared distribution for the $\tau^- \to \pi^-\pi^0\,\nu_\tau$ decay, $\mathcal{B}_e$ is the branching fraction for $\tau^- \to e^-\nu_\tau\bar{\nu}_e$ and $S_{\rm EW} = S^{\pi\pi}_{\rm EW}/S^e_{\rm EW}$.

In this paper, we report new measurements for both the branching fraction $\mathcal{B}_{\pi\pi}$ and the normalized mass spectrum $(1/N_{\pi\pi})({\rm d}N_{\pi\pi}/{\rm d}s)$. These results are used to provide a new evaluation of the hadronic contribution to the muon anomalous magnetic moment from the $2\pi$ channel.

## III. DATA SAMPLE AND SELECTION CRITERIA

The data sample used was collected with the Belle detector at the KEKB asymmetric-energy $e^+e^-$ collider [35]. It is based on an integrated luminosity of 72.2 fb$^{-1}$ recorded at a CM energy of 10.58 GeV. The Belle detector is a large-solid-angle magnetic spectrometer consisting of several detector components. Charged track coordinates near the collision point are measured by a three-layer silicon-vertex detector (SVD) that surrounds a 2 cm radius beryllium beam pipe. Track trajectory coordinates are reconstructed in a 50-layer central drift chamber (CDC), and momentum measurements are made together with the SVD. An array of 1188 silica-aerogel Cherenkov counters (ACC), a barrel-like arrangement of time-of-flight scintillation counters (TOF), and specific ionization measurements ($dE/dx$) in the CDC provide a capability for the identification of charged particles. Photon detection and energy measurement of the photons and electrons are provided by an electromagnetic calorimeter (ECL) consisting of an array of 8736 CsI(Tl) crystals all pointing toward the interaction point. These detector components are located in a magnetic field of 1.5 T provided by a superconducting solenoid. An iron flux-return located outside the coil is instrumented to identify muons and to detect $K_L^0$ mesons (KLM). A comprehensive description of the detector is given in Ref. [36].

To study backgrounds and determine selection criteria, we perform Monte Carlo (MC) simulation studies for various processes. Signal and background $\tau^+\tau^-$-pair events are simulated using the KKMC generator [37]. The $\tau$ decays are modeled with the TAUOLA program [38, 39] in which the values of the branching fractions are updated to more recent values [40]. The cross section for $e^+e^- \to \tau^+\tau^-(\gamma)$ is also updated to the recent measurement reported in Ref. [41]. The radiative corrections to the $\tau$-hadronic decays are simulated by the PHOTOS program [42]. The QQ generator [43] is used for $\bar{B}B$ and $\bar{q}q$ continuum processes, the BHLUMI [44] program for radiative Bhabha events, the KKMC [37] program for radiative $\mu^+\mu^-$-pair events, and the AAFH [45] program for two-photon processes. The BHLUMI and KKMC programs include higher-order radiative corrections and are among the most accurate programs available. The detector response is simulated by a GEANT3-based program [46]. In order to simulate beam-induced background realistically, detector hits taken from randomly triggered data are added to wire hits in the CDC and to energy deposits in the ECL. Uncertainties due to imperfections in the Monte Carlo generators and detector simulation are discussed in the later sections.

### A. $\tau^+\tau^-$ pair selection

The event selection consists of two steps. Initially, a sample of generic $e^+e^- \to \tau^+\tau^-(\gamma)$ events is selected with relatively loose criteria. From this sample $\tau^- \to \pi^-\pi^0\,\nu_\tau$ decays are identified. The number of generic $\tau^+\tau^-$ events is used to determine the $\tau^- \to \pi^-\pi^0\,\nu_\tau$ branching fraction.

Generic $\tau^+\tau^-$ events are selected by requiring that the number of charged tracks in an event be two or four with zero net charge; that each track have a momentum transverse to the beam axis ($p_T$) of greater than 0.1 GeV/$c$ to avoid tracks reentering the CDC; and that each track extrapolate to the interaction point (IP) within $\pm 1$ cm transversely and within $\pm 5$ cm along the beam direction to suppress tracks that originate from beam-particle interactions with the residual gas in the vacuum chamber. To suppress background from Bhabha and $\mu^+\mu^-$ events, the reconstructed CM energies and the sum of the momenta of

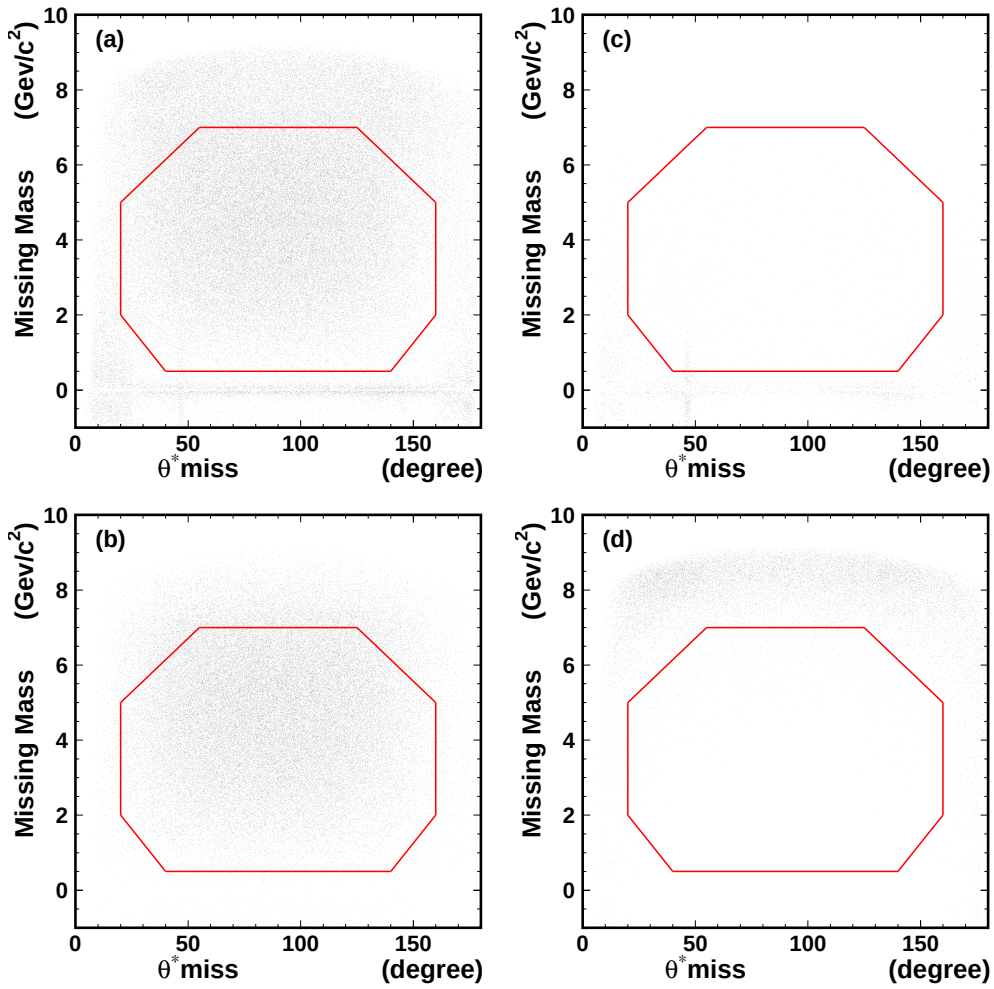


FIG. 1: Missing mass ($M_{\rm miss}$) versus the polar angle direction of the missing momentum ($\theta^*_{\rm miss}$) for (a) the data, (b) MC $e^+e^- \to \tau^+\tau^-$ events, (c) MC Bhabha and $\mu^+\mu^-(\gamma)$ events and (d) two-photon processes. Events inside the octagonal region are selected as $\tau^+\tau^-$-pair candidates.

the first and the second highest momentum tracks are required to be less than 9.0 GeV/$c$. The maximum $p_T$ among the tracks is required to be greater than 0.5 GeV/$c$. Beam-related background is rejected by requiring that the position of the reconstructed event vertex be less than 0.5 cm from the IP in the transverse direction and less than 2.5 cm from the IP along the beam direction. The polar angle of the leading particle with respect to the beam axis ($\theta^*$) in the CM frame is required to be in the fiducial region of the detector: $35^\circ < \theta^* < 145^\circ$.

To reduce the remaining background from Bhabha, $\mu^+\mu^-(\gamma)$, and two-photon events, a requirement is imposed in the plane of the missing mass $M_{\rm miss}$ and the direction of missing momentum in CM $\theta^*_{\rm miss}$, where $M_{\rm miss}$ is evaluated from the four-momenta of the measured tracks and photons: $(M_{\rm miss})^2 = (p_{\rm in} - p_{\rm tr} - p_\gamma)^2$. In this expression $p_{\rm in}$ is the four-momentum of the initial $e^+e^-$ system, while $p_{\rm tr}$ and $p_\gamma$ are the sum of the momenta of measured tracks and photons, respectively. A pion mass is assumed for the charged tracks if they are not identified as electrons or muons. Each photon (reconstructed from clusters in the calorimeter) must be separated from the nearest track projection by at least 20 cm

and have an energy greater than 0.05 GeV in the barrel region ($-0.63 \leq \cos\theta < 0.85$), and greater than 0.1 GeV in the endcap region ($-0.90 \leq \cos\theta < -0.62$ and $0.85 \leq \cos\theta < 0.95$). Photons near the edge of the detector fiducial volume are rejected. Scatter plots of $M_{\rm miss}$ versus $\theta_{\rm miss}$ for data, the $\tau$-signal MC, the Bhabha and the two-photon MC are shown in Figs. 1-(a), (b), (c) and (d), respectively. The band of events in data at $M_{\rm miss} \approx 0$ is due to backgrounds from Bhabha and $\mu^+\mu^-(\gamma)$ processes. Small vertical bands at $\theta^*_{\rm miss} = 45^\circ$ and $= 150^\circ$ are Bhabha events where the energy of one of the final state electron/positron is poorly measured because it has scattered in the material at the boundary of the barrel and endcap calorimeters. The events in the high-$M_{\rm miss}$ region ($\geq 7{\rm GeV}/c^2$) are from the two-photon processes.

Events within the octagonal region are selected as $\tau^+\tau^-$candidates to avoid the tail from background processes.

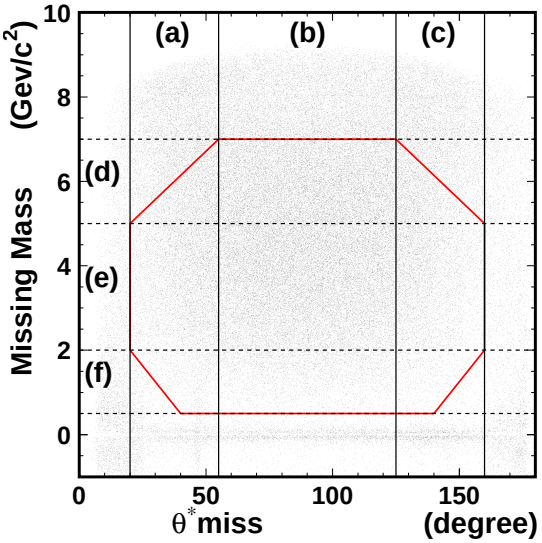


FIG. 2: Missing mass ($M_{\rm miss}$) versus the polar angle direction of the missing momentum ($\theta^*_{\rm miss}$) for data. The solid (dashed) lines show three vertical (horizontal) slices that are used to present the projections in Fig. 3. The coordinates of the vertical (horizontal) lines are $\theta^*_{\rm miss} = 20^\circ$, $55^\circ$, $125^\circ$, $160^\circ$ ($M_{\rm miss} = 0.5$ GeV/$c^2$, 2.0 GeV/$c^2$, 5.0 GeV/$c^2$, 7.0 GeV/$c^2$).

To display the $\tau$-pair and background contribution quantitatively, we divide the scatter plots of $M_{\rm miss}$ vs $\theta_{\rm miss}$ into three vertical and three horizontal slices as shown in Fig.2. Projections for the six slices are shown in Fig. 3, where each process shows a characteristic shape: the $\tau^+\tau^-$ candidates dominate in the central region in $M_{\rm miss}$ and $\theta^*_{\rm miss}$. Both Bhabha and $\mu^+\mu^-$ show a prominent peak at $M_{\rm miss} \approx 0$, but the width for the Bhabha is slightly wider than that of $\mu^+\mu^-$. We use the events in the region $|M_{\rm miss}| < 0.5$ GeV/$c^2$ to determine the normalization for the Bhabha and $\mu^+\mu^-$. As two-photon processes dominate in the high-$M_{\rm miss}$ region, the normalization for the two-photon processes is determined using the events at $|M_{\rm miss}| > 8.0$ GeV/$c^2$. The arrows with solid (dotted) lines indicate the narrowest (widest) areas used to select $\tau^+\tau^-$-pairs by the octagonal selection. Although overall features of the data are modeled reasonably well by MC, some discrepancies are seen, for example, in the regions $M_{\rm miss} \approx 0$ and $> 6$ GeV/$c^2$ in Fig 4-(c), which are taken into account as the systematic error on the background estimation.

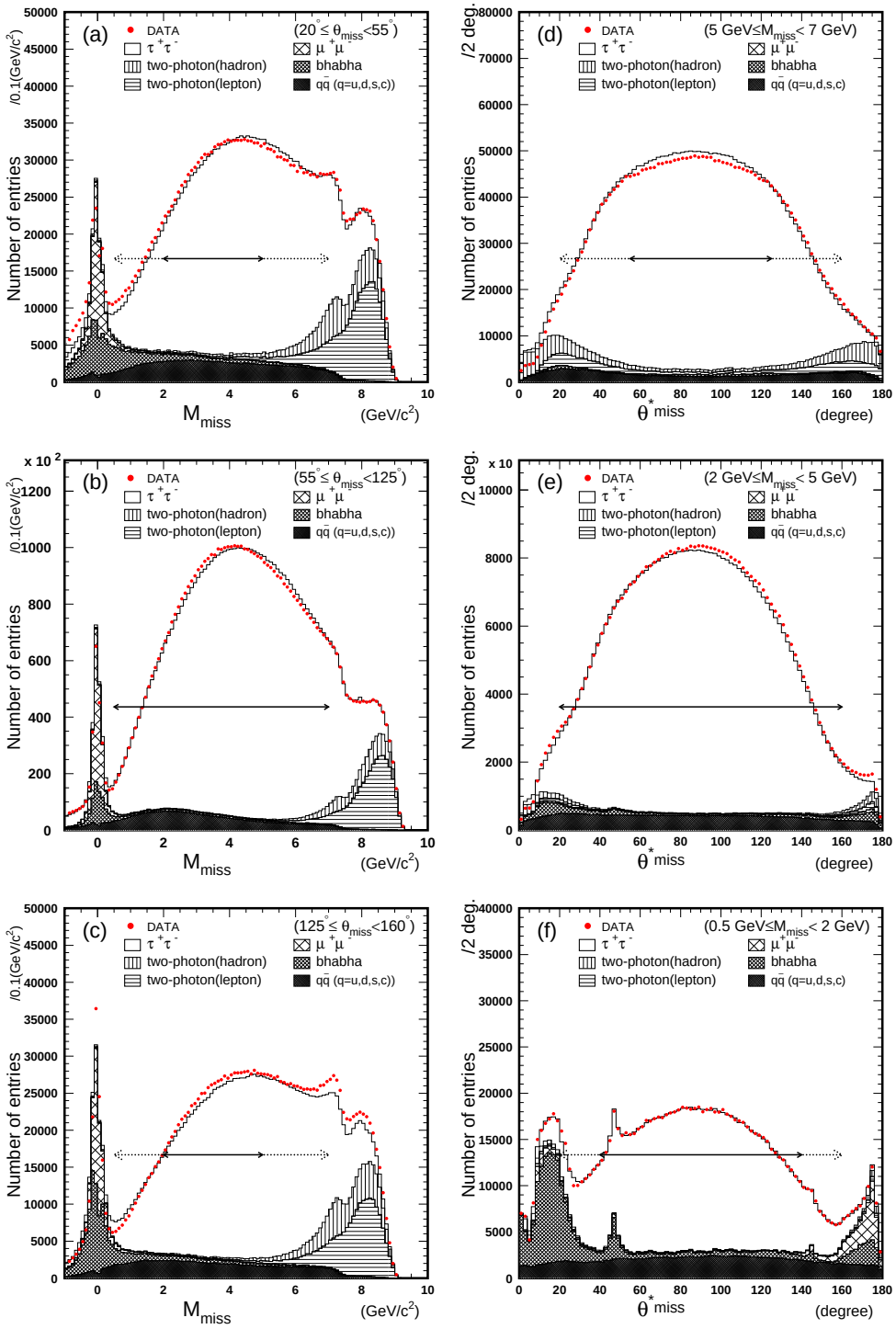


FIG. 3: Projections to the missing mass ($M_{\rm miss}$) and the missing direction ($\theta^*_{\rm miss}$): (a)-(c) correspond to the vertical slices from left to right in Fig.2. (d)-(f) correspond to the horizontal slices from top to bottom. The solid circles represent the data, and the histogram represents MC simulation (signal+ background). The open histogram shows the contribution from $\tau^+\tau^-$-pair process, the vertical (horizontal) striped area shows that from two-photon leptonic (hadronic) processes; the wide (narrow) hatched area shows that from Bhabha ($\mu^+\mu^-$) process; and the shaded area shows that from the $q\bar{q}$ continuum processes. The arrows with solid (dotted) lines indicates the widest (narrowest) region corresponding to the octagonal boundary shown in Fig 2.

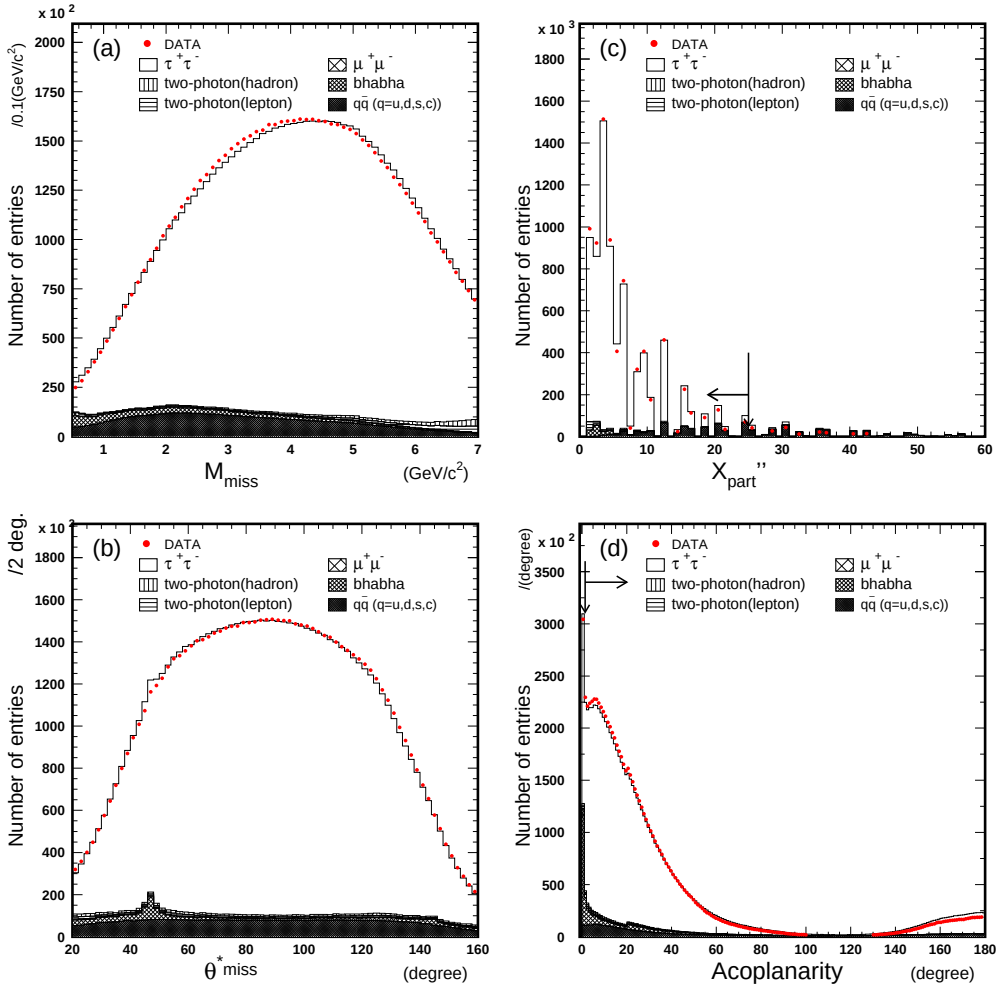


FIG. 4: Characteristic distributions for surviving $\tau^+\tau^-$ candidates: (a) $M_{\rm miss}$, (b) $\theta_{\rm miss}$, (c) particle multiplicity $X_{\rm part} \equiv (n_{\rm tr}+n_\gamma)_1 \times (n_{\rm tr}+n_\gamma)_2$, (d) acoplanarity angle $\xi$. The points indicate the data, the open histogram shows the $\tau$-pair MC and the hatched histogram shows the background from $e^+e^- \to q\bar{q}$ and other sources. All selection criteria are applied for (a) and (b). All criteria except for the quantity in question are applied for (c) and (d). The arrows in (c) and (d) indicate the boundary used to select a $\tau$-pair sample.

Candidate events are divided into two hemispheres in the CM frame by the plane perpendicular to the highest momentum particle, and the remaining background from $e^+e^-$ annihilation is suppressed by selecting events with low multiplicity as characterized by the quantity $X_{\rm part} \equiv (n_{\rm tr}+n_\gamma)_1 \times (n_{\rm tr}+n_\gamma)_2$, where $n_{{\rm tr},j}$ and $n_{\gamma,j}$ are the numbers of tracks and photons in hemisphere $j$. We require $X_{\rm part} \leq 25$. Finally, in order to eliminate Bhabha events in which one or both electrons produce a shower in material near the interaction region, the acoplanarity angle $\xi$ between the first and second highest momentum tracks is required to be $\xi > 1^\circ$, where $\xi \equiv ||\phi_1 - \phi_2| - \pi|$ is defined as the two-track acollinearity in azimuth. The $X_{\rm part}$ and $\xi$ distributions after applying all selection criteria except for the quantity in question are shown in Figs. 4-(c) and (d), respectively. The selection boundary is shown by the arrows.

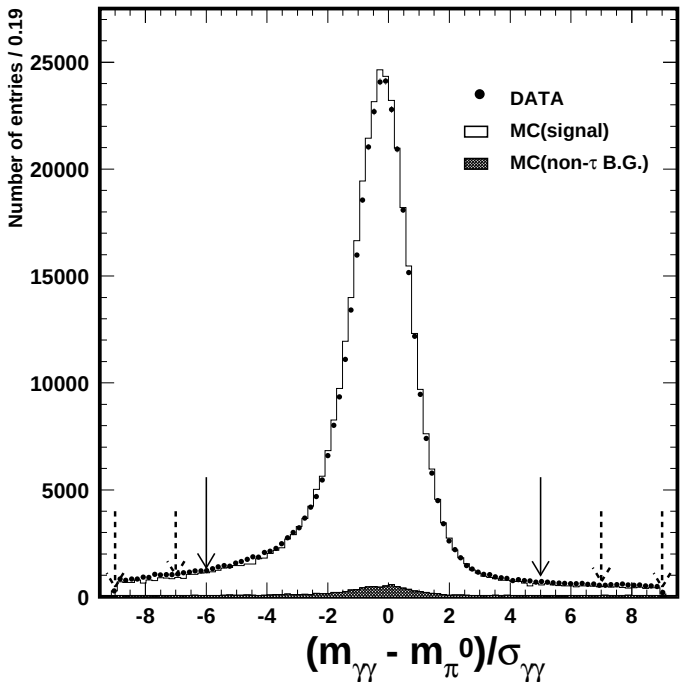


FIG. 5: Normalized $\gamma\gamma$ invariant mass ($S_{\gamma\gamma}$) spectrum for data (points) and the $\tau^-\to h^-\pi^0\,\nu_\tau$ signal MC (open histogram), for the sample described in the text. The data plotted here correspond to 6% of the full data sample used in this analysis. The arrows indicate the signal region $-6 < S_{\gamma\gamma} < 5$ and the sideband regions $7 < |S_{\gamma\gamma}| < 9$. The sideband regions are used to subtract fake-$\pi^0$ background. The shaded histogram shows the non-$\tau$ background determined from MC simulation.

After applying all selection criteria, $22.83 \times 10^6$ $\tau^+\tau^-$-pairs survive. The $M_{\rm miss}$ and $\theta_{\rm miss}$ distributions for the surviving events, shown in Fig.4-(a) and (b), respectively, demonstrate a low level of the background and an overall good agreement between the data and the MC model.

For surviving events, the dominant background is from the $e^+e^- \to q\bar{q}$ $(q = u, d, s, c)$ continuum and amounts to $(5.30 \pm 0.53)\%$ of the total number of events. The systematic error for the $q\bar{q}$ background is determined from the uncertainty of the normalization of the events in the region $25 < X_{\rm part} < 30$, where $q\bar{q}$ processes dominate. The background from $e^+e^- \to \Upsilon(4S) \to B\bar{B}$ is small (0.1 %). Backgrounds from Bhabha, $\mu^+\mu^-$, two-photon leptonic and hadronic events are to be $0.92 \pm 0.09$ %, $0.28 \pm 0.01\%$, $0.62 \pm 0.03\%$ and $0.60 \pm 0.09\%$, respectively. Here the systematic errors for each background is determined from the uncertainty of the normalization of the events in the background enhanced region mentioned before.

### B. $\tau^-\to\pi^-\pi^0\,\nu_\tau$ selection

Within the $\tau^+\tau^-$-pair sample, $\tau^-\to\pi^-\pi^0\,\nu_\tau$ decays are reconstructed by requiring that there be both one charged track and one $\pi^0$ in a single hemisphere. The $\pi^0$ candidate is selected based on the normalized invariant mass $S_{\gamma\gamma} \equiv (m_{\gamma\gamma} - m_{\pi^0})/\sigma_{\gamma\gamma}$, where $\sigma_{\gamma\gamma}$ is the

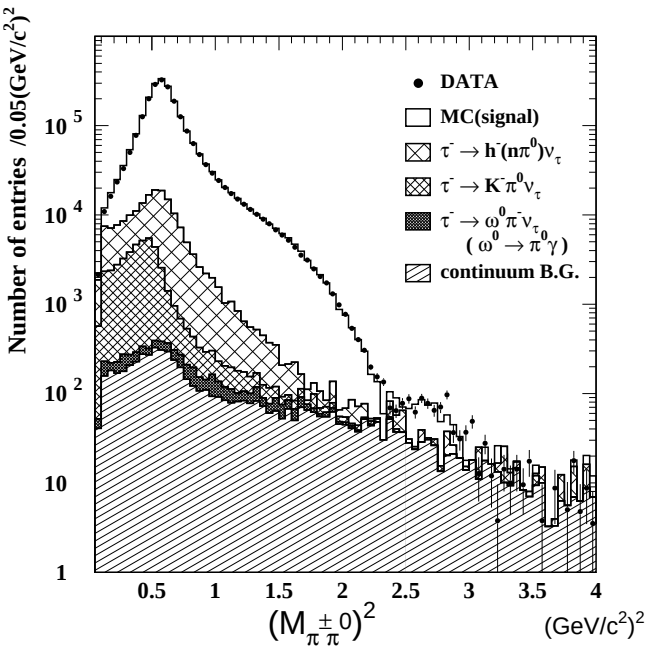


FIG. 6: Invariant-mass-squared ($M^2_{\pi\pi^0}$) distribution for $\tau^-\to\pi^-\pi^0\,\nu_\tau$ after imposing tight tag-side requirements. The solid circles with error bars represent the data, and the histogram represents the MC simulation (signal + background). The open histogram shows the contribution from $\tau^-\to\pi^-\pi^0\,\nu_\tau$; the narrow cross-hatched area shows that from $\tau^-\to K^-\pi^0\nu_\tau$; the wide cross-hatched area shows that from $\tau^-\to h^-(n\pi^0)\nu_\tau$; and the striped area shows that from the $q\bar{q}$ continuum and other non-$\tau$ processes.

mass resolution of the $\gamma\gamma$ system. The value of $\sigma_{\gamma\gamma}$ ranges from 0.005 GeV/$c^2$ to 0.008 GeV/$c^2$, depending on the $\pi^0$ momentum and polar angle. Pairs of photons with $|S_{\gamma\gamma}| < 9$ are considered as $\pi^0$ candidates. To keep beam-related background at a negligible level, we require that the CM momentum of the $\pi^0$ be greater than 0.25 GeV/$c$ and the photon CM energy be greater than 0.08 GeV.

The distribution of $S_{\gamma\gamma}$ for the selected $\pi^-\pi^0$ sample, with one charged track and one $\pi^0$ candidate in a single hemisphere, is shown in Fig. 5. The lower-side tail of the $S_{\gamma\gamma}$ distribution is primarily due to rear and transverse leakage of electromagnetic showers out of the CsI(Tl) crystals and the conversion of photons in the material located in front of the crystals. Good agreement between data (points) and MC (open histogram) indicates that these effects are properly modeled by the MC simulation. We define the interval $-6 < S_{\gamma\gamma} < 5$ as the $\pi^0$ signal region. Spurious $\pi^0$ background is small and estimated from the sideband regions $7 < |S_{\gamma\gamma}| < 9$. To reduce feed-down background from multi-$\pi^0$ decays such as $\tau^-\to\pi^-(n\pi^0)\nu_\tau$ ( $n \geq 2$), signal candidates are rejected if there are additional $\gamma$'s in the same hemisphere with energy greater than 0.2 GeV.

The $\pi^-\pi^0$ invariant-mass-squared ($M^2_{\pi\pi^0}$) spectrum is obtained assuming the pion mass for the charged track; it is shown in Fig. 6 along with the MC prediction. To improve the $\pi^0$ energy resolution, a $\pi^0$ mass constraint is imposed. The spurious $\pi^0$ background level depends on the $M^2_{\pi\pi^0}$ region, varying from 4% to 7%. (This is subtracted using $S_{\gamma\gamma}$

sidebands.) The final sample contains $5.43 \times 10^6$ $\tau^- \to h^-\pi^0\,\nu_\tau$ candidates after the $\pi^0$ background subtraction, where $h^-$ denotes $\pi^-$ or $K^-$. This sample is 50 times larger than those of previous studies.

The spectrum is dominated by the $\rho(770)$ peak and a shoulder due to the $\rho'(1450)$. A small but clear structure from the $\rho''(1700)$ is visible at $M^2_{\pi\pi^0} \sim 2.7$ (GeV/$c^2$)$^2$.

There are two sources of background: feed-down from other $\tau$ decay modes and the $q\bar{q}$-continuum. Feed-down background arises mainly from multi-$\pi^0$ modes such as $\tau^- \to h^-(n\pi^0)\nu_\tau$ ($6.02 \pm 0.08\%$), $\tau \to K_L h^-\pi^0\nu_\tau (0.48 \pm 0.04\%)$ and $\tau \to \omega\pi^-\nu_\tau(\omega \to \pi^0\gamma)$ ($0.10 \pm 0.01\%$). Here $h^-$ denotes either $\pi^-$ or $K^-$. After all modes are included, the total feed-down background level is $(7.02 \pm 0.08)\%$. The error given here includes a MC statistical uncertainty as well as the uncertainty on relevant branching fractions. The contribution of these feed-down backgrounds dominates at low values of $M^2_{\pi\pi^0}$ (Fig. 6).

The $q\bar{q}$-continuum background level is $(2.22 \pm 0.05)\%$ in total, and is concentrated mostly in the high $M^2_{\pi\pi^0}$ region above 2.0 (GeV/$c^2$)$^2$. Since the reduction of this high-mass background is essential in the measurement of the mass spectrum, we impose the stringent requirement that the tag side contain only one charged track and no photons. This requirement improves the signal-to-noise ratio in the high-mass region $M^2_{\pi\pi^0} \geq 2.0$ (GeV/$c^2$)$^2$ by a factor of 3, although the total size of the $\tau^- \to \pi^-\pi^0\,\nu_\tau$ sample is reduced by a factor of 2.5. The normalization of the continuum MC is validated using data in the mass region above the $\tau$ lepton mass: $M^2_{\pi\pi^0} > m^2_\tau$. Background from the other non-$\tau$ processes, such as $B\bar{B}$, Bhabha and $\mu^+\mu^-\gamma$ in the final sample is negligible ($< 0.1\%$).

## IV. MEASUREMENT OF THE BRANCHING FRACTION

### A. Basic Method

The branching fraction for $\tau^- \to h^-\pi^0\,\nu_\tau$ ($\mathcal{B}_{h\pi^0}$) is determined by dividing the signal yield $N_{h\pi^0}$ by the total number of selected $\tau$ leptons $2N_{\tau\tau}$ taking into account various efficiencies and background corrections:

$$\mathcal{B}_{h\pi^0} \;=\; \frac{N_{h\pi^0}}{2N_{\tau\tau}} \times \frac{(1 - b^{\text{feed-down}} - b^{\text{non-}\tau})}{(1 - b_{\tau\tau})} \times \left(\frac{\epsilon_{\tau\tau}}{\epsilon^{\tau}_{h\pi^0}}\right) \times \frac{1}{\epsilon^{ID}_{h\pi^0}}\,. \tag{8}$$

In this formula, $b_{\tau\tau}$ is the background fraction in the $\tau^+\tau^-$ sample, $\epsilon_{\tau\tau}$ is the efficiency of the $\tau^+\tau^-$-pair selection, $\epsilon^{\tau}_{h\pi^0}$ is the efficiency for $\tau^- \to h^-\pi^0\nu$ decays to pass the $\tau^+\tau^-$-pair selection, and $\epsilon^{ID}_{h\pi^0}$ is the efficiency for $\tau^- \to h^-\pi^0\nu$ decays satisfying the $\tau^+\tau^-$-pair selection to pass the $h^-\pi^0$ selection. The product $\epsilon^{\tau}_{h\pi^0} \cdot \epsilon^{ID}_{h\pi^0}$ is the overall detection efficiency for the $h^-\pi^0\nu$ final state. The parameter $b^{\text{feed-down}}$ is the fraction of $h^-\pi^0\nu$ candidates coming from other $\tau$ decay modes, and $b^{\text{non-}\tau}$ is the fraction coming from non-$\tau$ processes. In this formula, several common uncertainties such as that on the luminosity, on the cross section for $\tau^+\tau^-$-pair production, on the trigger efficiency, and on the $\tau^+\tau^-$ selection efficiency cancel in the ratio. In the measurement of the branching fraction, the stringent tag-side condition is not imposed to avoid any possible bias that it might introduce. The values for all factors are listed in Table I along with the MC statistical error.

TABLE I: Values of parameters used for the branching fraction measurement along with MC statistical errors.

| Parameter | Value |
|---|---|
| $\varepsilon_{\tau\tau}$ | $32.59 \pm 0.05$ % |
| $\varepsilon^{\tau}_{h\pi^0}$ | $36.24 \pm 0.07$ % |
| $f_b = \frac{\varepsilon^{\tau}_{h\pi^0}}{\varepsilon_{\tau\tau}}$ | $1.112 \pm 0.003$ |
| $\varepsilon^{ID}_{h\pi^0}$ | $41.01 \pm 0.13$ % |
| $b_{\tau\tau}$ | $7.80 \pm 0.03$ % |
| $b^{\text{feed-down}}_{h\pi^0}$ | $7.02 \pm 0.08$ % |
| $b^{\text{non-}\tau}_{h\pi^0}$ | $2.22 \pm 0.05$ % |

### B. Systematic uncertainties

The sources of systematic uncertainties on $\mathcal{B}_{h\pi^0}$ are listed in Table II. The uncertainty on the tracking efficiency is estimated using $D^{*+} \to D^0\pi^+ \to K^-\pi^+\pi^+$ decays to be 1% per track. A large part of this uncertainty cancels in the ratio of Eq. (8); the resulting relative uncertainty from this source is $\Delta\mathcal{B}/\mathcal{B} = 0.47$ %.

TABLE II: Systematic uncertainties for the $\tau^- \to h^-\pi^0\,\nu_\tau$ branching fraction.

| Source of uncertainty | $\Delta\mathcal{B}_{h\pi^0}$ (%) | $(\Delta\mathcal{B}/\mathcal{B})$ (%) |
|---|---|---|
| Tracking efficiency | 0.12 | 0.47 |
| $\pi^0$ efficiency | 0.32 | 1.27 |
| Background for $\tau^+\tau^-$ | 0.15 | 0.59 |
| Feed-down background for $\tau^- \to h^-\pi^0\,\nu_\tau$ | 0.04 | 0.16 |
| Non-$\tau$ background for $\tau^- \to h^-\pi^0\,\nu_\tau$ | 0.05 | 0.20 |
| $\gamma$ veto | 0.05 | 0.20 |
| Trigger | 0.08 | 0.32 |
| MC statistics | 0.02 | 0.08 |
| Total | 0.39 | 1.52 |

The systematic error on the $\pi^0$ detection efficiency has two components: one is the uncertainty coming from the $\pi^0$ selection criteria and the other is that from the absolute efficiency calibration. For the uncertainty coming from the $\pi^0$ selection, we check the uncertainty by changing the definition of the signal and background region, by taking into account the uncertainty in the resolution function and by changing the $\pi^0$ threshold momentum. For example, the relative branching fraction changes by only $\Delta\mathcal{B}/\mathcal{B} = 0.1\%$ if the signal region is changed from the nominal one to $-7 < S_{\gamma\gamma} < 7$. Also the uncertainty is $\Delta\mathcal{B}/\mathcal{B} = \pm 0.2\%$ for the changes of the $\pi^0$ threshold by $\pm 0.05$ GeV from the nominal value.

In order to make an absolute efficiency calibration independently of the signal process, we use the $\eta \to \gamma\gamma$ and $\eta \to \pi^0\pi^0\pi^0$ signals, whose branching fractions are known rather precisely. Combining the PDG world average [31] for the $\eta \to \gamma\gamma$ and $\eta \to \pi^0\pi^0\pi^0$ branching fractions and the recent measurement from the CLEO collaboration [47], we obtain the ratio of the branching fractions of

$$\frac{\mathcal{B}(\eta \to \gamma\gamma)}{\mathcal{B}(\eta \to \pi^0\pi^0\pi^0)} = 0.829 \pm 0.007,$$

which has 0.84% relative accuracy.

By comparing the signal ratio $R_i \equiv N(\eta \to \pi^0\pi^0\pi^0/N(\eta \to \gamma\gamma))$ for the data ($i = 1$) and the MC ($i = 2$), the correction factor for the detection efficiency of one $\pi^0$, $\eta_{\rm cor}$, is determined to be $\eta_{\rm cor} = \sqrt{R_{\rm data}/R_{\rm MC}} = 0.950 \pm 0.012$, where the error includes the uncertainties in the $\eta$ signal measurement (1.2%) and the errors on the $\eta$ decay branching fractions (0.4%).

This correction factor is also confirmed by a study of electron/positron tracks from photon conversions (i.e. $\gamma \to e^+e^-$) in the SVD region. It is found that the $E/P$ distribution for those tracks is simulated correctly above 1.0 GeV, but requires some tuning below 1.0 GeV. This imperfection of the MC primarily leads to a difference in the $\pi^0$ signal shape and an efficiency difference between data and MC.

The non-$\tau$ background is dominated by $q\bar{q}$ continuum processes; this is estimated by using the events above the $\tau$ mass: $M^2_{\pi\pi^0} > m^2_\tau$. The statistics of the data and MC sample determine the error.

The uncertainty on the feed-down background $\Delta b^{\rm feed-down}_{h\pi^0}$ comes from the MC statistics and the uncertainty on the branching fractions for $\tau^- \to h^-(n\pi^0)\nu_\tau$, $\tau^- \to K^-\pi^0\nu_\tau$ and $\tau^- \to \omega\pi^-\nu_\tau$ ($\omega \to \pi^0\gamma$).

The veto of additional $\gamma$'s is required in the event selection to reduce background from multi-$\pi^0$ decay channels. However, this veto can reject signal itself if photons are radiated in the initial or final state and those photons are detected within the detector fiducial volume. In addition, photon candidates can also appear due to electromagnetic shower fragments and/or misreconstructed electrons. Therefore a precise simulation of the photon radiation as well as the shower simulation are important. The uncertainty from these sources is estimated by changing the veto threshold by $\pm 0.1$ GeV around the nominal value of 0.2 GeV; the resulting relative change in $\mathcal{B}_{h\pi^0}$ is only $\pm 0.20\%$. Signal events are flagged by several trigger conditions that require two or more CDC tracks with associated TOF hits, ECL clusters, or a significant sum of energy in the ECL. This redundancy allows one to monitor the efficiency of each trigger requirement. The uncertainty arising from the trigger is estimated by assuming that there is a $\pm 3\%$ uncertainty on the track and energy trigger efficiencies, which is the maximum variation measured during experimental running. The resulting relative uncertainty is small (0.32%) since the $\tau^+\tau^-$ trigger efficiency is high (97%).

### C. Results

Inserting all values into Eq. (8) we obtain

$$\mathcal{B}_{h\pi^0} \;=\; (25.67 \,\pm\, 0.01 \,\pm\, 0.39)\%\,, \tag{9}$$

where the first error is statistical and the second is systematic. This result is in good agreement with previous measurements, as shown in Table III. Our statistical error is

significantly lower than those of the other measurements; our systematic error is similar to those of CLEO, L3 and OPAL, and larger than those of ALEPH and DELPHI.

TABLE III: Branching fractions for $\tau^- \to h^- \pi^0 \, \nu_\tau$ measured by different experiments.

| Experiment | $\mathcal{B}_{h\pi^0}(\%)$ | Reference |
|---|---|---|
| CLEO | $25.87 \pm 0.12 \pm 0.42$ | [21] |
| L3 | $25.05 \pm 0.35 \pm 0.50$ | [24] |
| OPAL | $25.89 \pm 0.17 \pm 0.29$ | [23] |
| ALEPH | $25.924 \pm 0.097 \pm 0.085$ | [19] |
| DELPHI | $25.740 \pm 0.201 \pm 0.138$ | [25] |
| This work | $25.67 \pm 0.01 \pm 0.39$ | |

We combine the PDG world average for the $\tau^- \to K^- \pi^0 \nu_\tau$ branching fraction [31] with a recent BaBar measurement [48] to obtain the result $\mathcal{B}_{K^-\pi^0} = (0.428 \pm 0.015)\%$. Subtracting this from our $\tau^- \to h^- \pi^0 \, \nu_\tau$ result gives a $\tau^- \to \pi^- \pi^0 \, \nu_\tau$ branching fraction of

$$\mathcal{B}_{\pi\pi^0} \; = \; (25.24 \; \pm \; 0.01 \; \pm \; 0.39)\% \, , \tag{10}$$

which is consistent with the previous measurements from CLEO [21] and ALEPH [19].

## V. MEASUREMENT OF THE MASS SPECTRUM

In order to obtain the true $\pi^-\pi^0$ mass spectrum, one must apply corrections for: (1) background, (2) smearing due to finite resolution and radiative effects, and (3) mass-dependent acceptance.

### A. Background Correction

As noted earlier, there are three sources of the background that enter the $\tau^- \to \pi^- \pi^0 \, \nu_\tau$ sample: (1) fake $\pi^0$ background, (2) feed-down background from other $\tau$ decay channels, and (3) the background from the $q\bar{q}$ continuum. The total magnitude of these background contributions is about 7% in the $\rho(770)$) peak region, but the fraction of the background varies strongly with $M^2_{\pi\pi^0}$; there is approximately a 4-order-of-magnitude difference between the signal level in the $\rho(770)$ peak region and that in the high $M^2_{\pi\pi^0}$ region above 2.5 $(\mathrm{GeV}/c^2)^2$. Thus a reliable estimation of the background is important for the measurement of the mass spectrum.

The sidebands of the $M_{\gamma\gamma}$ distribution are used to estimate the fake $\pi^0$ contribution. This background dominates at values of $M^2_{\pi\pi^0}$ less than about 0.25 $(\mathrm{GeV}/c^2)^2$.

In the $\pi^-\pi^0$ system, the feed-down background dominates at similarly low values of $M^2_{\pi\pi^0}$ while the $q\bar{q}$-continuum background dominates at high values of $M^2_{\pi\pi^0}$ (see Fig. 6). These backgrounds are subtracted bin-by-bin.

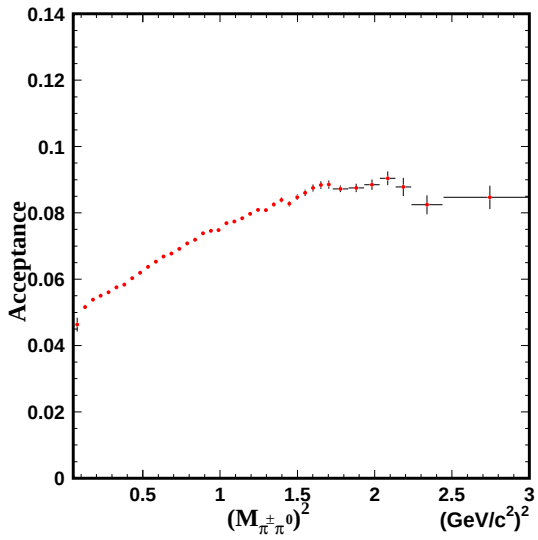


FIG. 7: The acceptance determined from MC simulation as a function of the $\pi^-\pi^0$ mass squared.

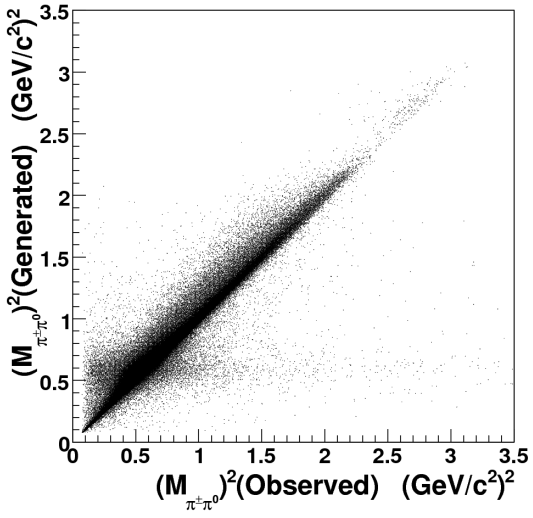


FIG. 8: Correlation between the generated and observed invariant masses squared of the $\pi^-\pi^0$ system in the $\tau^-\to\pi^-\pi^0\,\nu_\tau$ decay.

### B. Acceptance Correction

The acceptance determined from MC simulation as a function of the generated $\pi^-\pi^0$ mass squared is shown in Fig. 7. The acceptance varies smoothly and its average value is 7%. This acceptance includes a factor for the tag-side branching fractions $\mathcal{B}(\tau^-\to\ell^-\bar{\nu}_\mu\nu_\tau)$ $(\ell^- = \mu^-, e^-)$, $\mathcal{B}(\tau^-\to h^-\nu_\tau)$ $(h^- = \pi^-, K^-)$, which does not affect the shape of the mass spectrum. The acceptance decreases at low values of $M^2_{\rm gen}$ due to the overlap of $\gamma$ clusters with the $\pi^-$ track in the calorimeter.

The detector effects include $M^2_{\pi\pi^0}$-dependent acceptance and bin-by-bin migration caused by the finite mass resolution. The radiative decay $\tau^- \to \pi^-\pi^0\gamma\nu_\tau$ also causes some bin migration. We correct for these effects using an unfolding procedure that makes use of the MC to characterize the acceptance and the bin migration. These effects can be characterized by the acceptance matrix $A$ defined by

$$\boldsymbol{b} = A\,\boldsymbol{x}\,,$$

where $\boldsymbol{x}$ is the vector containing the generated $\pi^-\pi^0(\gamma)$ mass-squared spectrum and $\boldsymbol{b}$ is the reconstructed one. It is possible to apply the inverse of $A$ to the spectrum observed in the data to obtain an unfolded spectrum. However, this procedure is not robust with respect to the statistical fluctuations entering the determination of $A$, and can yield unphysically large point-by-point fluctuations. To cure this problem, we use an unfolding program employed in the ALEPH experiment [49]. In this program, the unfolding is based on the Singular-Value-Decomposition (SVD) method, in which the acceptance matrix is inverted by constraining the number of singular values to only those elements that are statistically significant.

The acceptance matrix is determined iteratively using a signal MC based on the KKMC/TAUOLA program. In the second iteration, the $\rho''(1700)$ resonance is included in the MC based on our measurement. Final state radiation in $\tau$ hadronic decays is simulated by the PHOTOS program. In order to take into account the effects of $\gamma$ radiation in the decay $\tau^- \to \pi^-\pi^0\gamma\nu_\tau$, the invariant mass squared of the $\pi^-\pi^0\gamma$ system is taken as the generated quantity.

The output of the program is the unfolded distribution and its covariance matrix. The correlation between the generated quantity and the measured one is shown in Fig. 8. The figure shows a clear correlation between the measured and generated values. The resolution in $M^2_{\pi\pi^0}$ is 0.005 $(\mathrm{GeV}/c^2)^2$ in the low-mass region and 0.030 $(\mathrm{GeV}/c^2)^2$ in the high-mass region; thus by choosing the bin size to be $\Delta M^2 = 0.050$ $(\mathrm{GeV}/c^2)^2$, the off-diagonal components of the acceptance matrix are small.

### C. Systematic Uncertainties

The sources of systematic errors associated with the unfolded mass spectrum $(1/N)(\mathrm{d}n/\mathrm{d}s)$ are subdivided into several classes according to their origin, which are the unfolding procedure (UNF), the background subtraction (BKG), the acceptance correction (ACC), and the energy scale (ENG). These contributions are summarized in Table IV for each $M^2_{\pi\pi^0}$ region and are described below.

The systematic error due to the unfolding procedure is determined from MC by comparing the true and the unfolded results (UNF1). Another estimate of the uncertainty of the unfolding is made by changing the value of the unfolding parameter that determines the optimum number of the singular values of the acceptance matrix (UNF2).

The uncertainty of the background subtraction is estimated for each source. BKG1 is from continuum processes. Its uncertainty is estimated using the control sample in the mass region higher than the $\tau$ mass. The statistics of the data and MC sample determine its error. BKG2 is the feed-down background. Its uncertainty is estimated by varying the branching fraction values [31] used in the MC by $\pm 1\sigma$. BKG3 is the non-$\pi^0$ background. The uncertainty of the non-$\pi^0$ background is estimated by changing the $\pi^0$ sideband region. This uncertainty dominates in the threshold region but is negligible elsewhere.

TABLE IV: Relative systematic errors (in %) of the unfolded spectrum for each $M^2_{\pi\pi^0}$ region for the different sources of uncertainty: unfolding procedure (UNF1, UNF2), the background subtraction (BKG1, BKG2, BKG3), the acceptance correction (ACC), and the photon energy scale (PES). See the text for a more detailed description.

| $M^2_{\pi\pi^0}$ region | First bin | Threshold region | $\rho$ region | | $\rho'$ region | $\rho''$ region |
|---|---|---|---|---|---|---|
| $((\mathrm{GeV}/c^2)^2)$ | (0.08) | (0.2-0.3) | (0.55-0.60) | (1.0-1.2) | (1.9-2.0) | (2.5-2.7) |
| UNF1 | 2.50 | 0.79 | 0.31 | 0.85 | 1.50 | 1.50 |
| UNF2 | 2.60 | 0.53 | 0.09 | 0.27 | 0.58 | 9.19 |
| BKG1 | 1.13 | 0.09 | 0.01 | 0.04 | 0.52 | 5.76 |
| BKG2 | 4.90 | 0.65 | 0.10 | 0.10 | ... | 0.50 |
| BKG3 | 25.21 | 4.80 | ... | ... | ... | ... |
| ACC | 5.36 | 1.44 | 0.03 | 0.15 | 0.15 | 0.40 |
| PES | 1.24 | 1.08 | 0.59 | 0.99 | 0.05 | 0.50 |
| Total | 26.5 | 5.3 | 0.7 | 1.5 | 1.8 | 11.4 |

The acceptance uncertainty is dominated by the uncertainty of the $\pi^0$ efficiency. This is estimated by changing the measured values of the photon efficiency by 1 standard deviation. In addition, the effect of requiring that photons be isolated from charged tracks is checked by changing the isolation criteria from 20 cm (default) to 30 cm.

The uncertainty of the photon energy scale (PES) is estimated from the $\pi^0$ peak position to be $\pm 0.2\%$. This uncertainty is important for the peak position of the resonances. The uncertainty in the charged track momentum scale is negligible compared to that of the photon energy scale.

Individual components of the uncertainty are added in quadrature to obtain total systematic errors of 5.3% in the threshold region, 0.7% near the $\rho(770)$ peak and 1.8% in the vicinity of the $\rho''(1450)$ (see Table IV).

### D. Results

The unfolded $s = M^2_{(\pi\pi^0\,\mathrm{unf.})}$ spectrum $\mathrm{d}N_{\pi\pi}/\mathrm{d}s$ is shown in Fig. 9. The error bars in the figure include both statistical and systematic errors added in quadrature and in most cases they are smaller than the size of the data points shown by closed circles. The results are also presented in terms of the normalized unfolded spectrum $(1/N_{\pi\pi})(\mathrm{d}N_{\pi\pi}/\mathrm{d}s)$ in Table V and in terms of the pion form factor in Table VI. In these tables, the statistical and systematic errors are given separately. The statistical errors in the figure and the table are the square roots of the diagonal components of the covariance matrix.

In Fig. 9, the $\rho$ peak and a shoulder due to the $\rho'(1450)$ are clearly visible. The dip at $s \approx 2.5$ $(\mathrm{GeV}/c^2)^2$ is caused by destructive interference between the $\rho'(1450)$ and $\rho''(1700)$ resonances.

To determine the parameters of the $\rho$, $\rho'$ and $\rho''$ resonances, a $\chi^2$ fit using Breit-Wigner (BW) functions is performed. The pion form factor is parametrized with Breit-Wigner

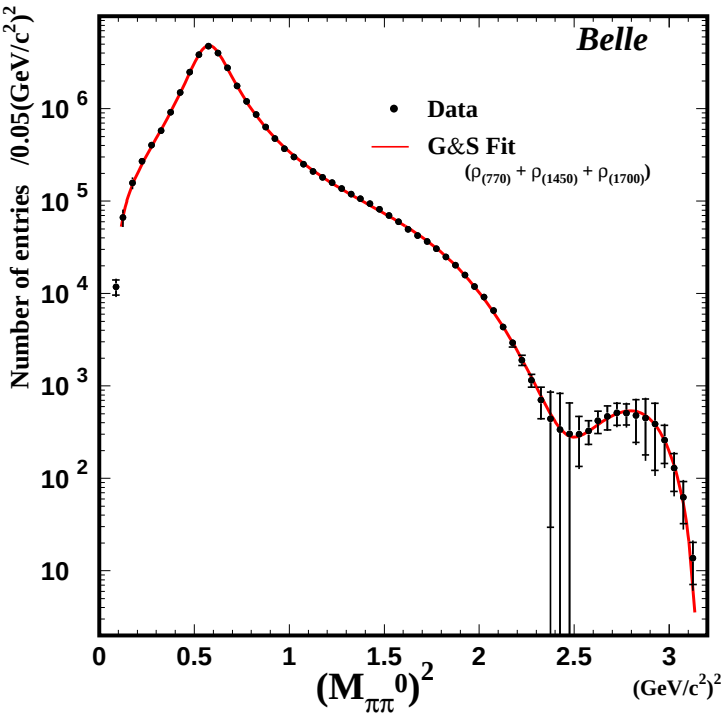


FIG. 9: The fully corrected $M^2_{\pi\pi^0}$ distribution for $\tau^- \to \pi^-\pi^0\,\nu_\tau$. The solid curve is the result of a fit to the Gounaris-Sakurai model with the $\rho(770)$, $\rho'(1450)$, and $\rho''(1700)$ resonances. All resonance parameters (mass, width, phase and the normalization factor $|F_\pi(0)|^2$) are allowed to float.

functions corresponding to the $\rho$, $\rho'(1450)$, and $\rho''(1700)$ resonances:

$$F_\pi(s) = \frac{1}{1+\beta+\gamma}(BW_\rho + \beta \cdot BW_{\rho'} + \gamma \cdot BW_{\rho''})\,, \tag{11}$$

where the parameters $\beta$ and $\gamma$ (denoting the relative magnitude of the two resonances) are in general complex. We use the Gounaris-Sakurai (GS) model [50] for the Breit-Wigner shape:

$$BW_i^{GS} = \frac{M_i^2 + d \cdot M_i\Gamma_i(s)}{(M_i^2 - s) + f(s) - i\sqrt{s}\Gamma_i(s)}\,, \tag{12}$$

with an energy-dependent width

$$\Gamma_i(s) = \Gamma_i \left(\frac{M_i^2}{s}\right)\left(\frac{k(s)}{k(M_i^2)}\right)^3\,. \tag{13}$$

Here, $k(s) = \frac{1}{2}\sqrt{s}\beta_-(s)$ is the pion momentum in the $\pi^-\pi^0$ rest frame. The functions $f(s)$ and $h(s)$ are defined as

$$f(s) \;=\; \Gamma_i \frac{M_i^2}{k^3(M_i^2)}\left[k^2(s)\left(h(s) - h(M_i^2)\right) + (M_i^2 - s)k^2(M_i^2)\left.\frac{dh}{ds}\right|_{s=M_i^2}\right] \tag{14}$$

TABLE V: The unfolded normalized spectrum $(1/N_{\pi\pi})(\mathrm{d}N_{\pi\pi}/\mathrm{d}s)$ as a function of the invariant mass squared $s = M^2_{\pi\pi^0}$. The square of the diagonal element of the error matrix is taken for the statistical errors. Note that the scale is different for the left-and right-sides.

| Bin No. | $M^2_{\pi\pi^0}$ $(\mathrm{GeV}/c^2)^2$ | $\frac{1}{N}\frac{\mathrm{d}N}{\mathrm{d}s}$ $\times 10^{-3}$ $\mathrm{GeV}^{-2}c^4$ | Stat. $\times 10^{-3}$ $\mathrm{GeV}^{-2}c^4$ | Syst. $\times 10^{-3}$ $\mathrm{GeV}^{-2}c^4$ | Bin No. | $M^2_{\pi\pi^0}$ $(\mathrm{GeV}/c^2)^2$ | $\frac{1}{N}\frac{\mathrm{d}N}{\mathrm{d}s}$ $\times 10^{-4}$ $\mathrm{GeV}^{-2}c^4$ | Stat. $\times 10^{-4}$ $\mathrm{GeV}^{-2}c^4$ | Syst. $\times 10^{-4}$ $\mathrm{GeV}^{-2}c^4$ |
|---|---|---|---|---|---|---|---|---|---|
| 1 | 0.088 | 8.1 | 3.1 | 2.1 | 32 | 1.625 | 341.47 | 5.91 | 5.83 |
| 2 | 0.125 | 45.8 | 2.4 | 9.6 | 33 | 1.675 | 290.94 | 5.56 | 5.39 |
| 3 | 0.175 | 108.4 | 2.4 | 15.5 | 34 | 1.725 | 250.39 | 4.99 | 4.32 |
| 4 | 0.225 | 185.1 | 2.6 | 14.3 | 35 | 1.775 | 210.22 | 4.86 | 3.40 |
| 5 | 0.275 | 278.0 | 2.8 | 8.3 | 36 | 1.825 | 170.63 | 4.36 | 2.75 |
| 6 | 0.325 | 396.0 | 3.3 | 4.1 | 37 | 1.875 | 139.72 | 3.89 | 2.26 |
| 7 | 0.375 | 628.6 | 4.2 | 5.0 | 38 | 1.925 | 109.26 | 3.82 | 1.85 |
| 8 | 0.425 | 1024.2 | 5.5 | 14.7 | 39 | 1.975 | 81.85 | 3.20 | 1.39 |
| 9 | 0.475 | 1710.8 | 7.2 | 21.5 | 40 | 2.025 | 63.08 | 2.84 | 1.25 |
| 10 | 0.525 | 2643.0 | 9.0 | 22.5 | 41 | 2.075 | 45.02 | 2.72 | 0.89 |
| 11 | 0.575 | 3268.0 | 9.7 | 21.4 | 42 | 2.125 | 29.89 | 2.22 | 0.65 |
| 12 | 0.625 | 2755.5 | 9.0 | 19.4 | 43 | 2.175 | 20.06 | 1.94 | 0.61 |
| 13 | 0.675 | 1907.2 | 7.4 | 17.0 | 44 | 2.225 | 13.08 | 1.68 | 0.42 |
| 14 | 0.725 | 1214.0 | 5.8 | 8.4 | 45 | 2.275 | 7.93 | 1.25 | 0.42 |
| 15 | 0.775 | 826.4 | 4.6 | 10.7 | 46 | 2.325 | 4.85 | 1.82 | 0.51 |
| 16 | 0.825 | 592.8 | 3.6 | 8.6 | 47 | 2.375 | 3.04 | 2.84 | 1.39 |
| 17 | 0.875 | 435.6 | 2.9 | 3.5 | 48 | 2.425 | 2.32 | 3.36 | 1.17 |
| 18 | 0.925 | 327.5 | 2.4 | 4.6 | 49 | 2.475 | 2.09 | 2.39 | 0.76 |
| 19 | 0.975 | 253.7 | 2.1 | 3.7 | 50 | 2.525 | 2.07 | 1.14 | 0.37 |
| 20 | 1.025 | 206.3 | 1.8 | 2.7 | 51 | 2.575 | 2.24 | 0.64 | 0.19 |
| 21 | 1.075 | 172.5 | 1.5 | 3.6 | 52 | 2.625 | 2.88 | 0.78 | 0.17 |
| 22 | 1.125 | 144.0 | 1.3 | 1.4 | 53 | 2.675 | 3.22 | 0.94 | 0.33 |
| 23 | 1.175 | 124.0 | 1.2 | 3.7 | 54 | 2.725 | 3.52 | 0.95 | 0.51 |
| 24 | 1.225 | 108.7 | 1.1 | 3.3 | 55 | 2.775 | 3.49 | 0.89 | 0.57 |
| 25 | 1.275 | 94.0 | 1.0 | 1.0 | 56 | 2.825 | 3.29 | 1.60 | 0.62 |
| 26 | 1.325 | 82.0 | 0.9 | 2.4 | 57 | 2.875 | 3.09 | 1.86 | 0.80 |
| 27 | 1.375 | 72.6 | 0.9 | 1.3 | 58 | 2.925 | 2.65 | 1.81 | 0.65 |
| 28 | 1.425 | 64.5 | 0.8 | 1.8 | 59 | 2.975 | 1.79 | 0.79 | 0.43 |
| 29 | 1.475 | 56.1 | 0.8 | 1.8 | 60 | 3.025 | 0.88 | 0.39 | 0.22 |
| 30 | 1.525 | 48.0 | 0.7 | 1.4 | 61 | 3.075 | 0.43 | 0.20 | 0.12 |
| 31 | 1.575 | 41.1 | 0.6 | 0.7 | 62 | 3.125 | 0.09 | 0.04 | 0.03 |

TABLE VI: The form factor squared $|F_\pi^-(s)|^2$ as a function of the invariant mass squared $s$. The results are obtained by inserting the measured value $(1/N_{\pi\pi})(\mathrm{d}N_{\pi\pi}/\mathrm{d}s)$ into Eq. (7). Note that the short-distance radiative correction is already applied, where the value of $S_{\rm EW}$ is taken to be $1.0235 \pm 0.0003$ (see the discussion in the Appendix).

| Bin No. | $M^2_{\pi\pi^0}$ $(\mathrm{GeV}/c^2)^2$ | $\lvert F_\pi\rvert^2$ | Stat. | Syst. | Bin No. | $M^2_{\pi\pi^0}$ $(\mathrm{GeV}/c^2)^2$ | $\lvert F_\pi\rvert^2$ | Stat. | Syst. |
|---|---|---|---|---|---|---|---|---|---|
| 1 | 0.088 | 1.434 | 0.549 | 0.377 | 32 | 1.625 | 0.711 | 0.012 | 0.012 |
| 2 | 0.125 | 1.707 | 0.091 | 0.358 | 33 | 1.675 | 0.636 | 0.012 | 0.012 |
| 3 | 0.175 | 2.362 | 0.053 | 0.337 | 34 | 1.725 | 0.576 | 0.011 | 0.010 |
| 4 | 0.225 | 3.211 | 0.045 | 0.248 | 35 | 1.775 | 0.511 | 0.012 | 0.008 |
| 5 | 0.275 | 4.260 | 0.042 | 0.127 | 36 | 1.825 | 0.439 | 0.011 | 0.007 |
| 6 | 0.325 | 5.622 | 0.046 | 0.058 | 37 | 1.875 | 0.382 | 0.011 | 0.006 |
| 7 | 0.375 | 8.492 | 0.057 | 0.067 | 38 | 1.925 | 0.318 | 0.011 | 0.005 |
| 8 | 0.425 | 13.392 | 0.072 | 0.193 | 39 | 1.975 | 0.255 | 0.010 | 0.004 |
| 9 | 0.475 | 21.894 | 0.093 | 0.275 | 40 | 2.025 | 0.211 | 0.009 | 0.004 |
| 10 | 0.525 | 33.384 | 0.113 | 0.284 | 41 | 2.075 | 0.162 | 0.010 | 0.003 |
| 11 | 0.575 | 40.996 | 0.122 | 0.269 | 42 | 2.125 | 0.117 | 0.009 | 0.003 |
| 12 | 0.625 | 34.503 | 0.112 | 0.243 | 43 | 2.175 | 0.085 | 0.008 | 0.003 |
| 13 | 0.675 | 23.936 | 0.093 | 0.214 | 44 | 2.225 | 0.060 | 0.008 | 0.002 |
| 14 | 0.725 | 15.324 | 0.074 | 0.106 | 45 | 2.275 | 0.040 | 0.006 | 0.002 |
| 15 | 0.775 | 10.525 | 0.058 | 0.137 | 46 | 2.325 | 0.027 | 0.010 | 0.003 |
| 16 | 0.825 | 7.637 | 0.047 | 0.111 | 47 | 2.375 | 0.019 | 0.018 | 0.009 |
| 17 | 0.875 | 5.693 | 0.038 | 0.046 | 48 | 2.425 | 0.017 | 0.024 | 0.008 |
| 18 | 0.925 | 4.350 | 0.032 | 0.061 | 49 | 2.475 | 0.017 | 0.019 | 0.006 |
| 19 | 0.975 | 3.435 | 0.028 | 0.050 | 50 | 2.525 | 0.019 | 0.011 | 0.003 |
| 20 | 1.025 | 2.851 | 0.024 | 0.037 | 51 | 2.575 | 0.024 | 0.007 | 0.002 |
| 21 | 1.075 | 2.439 | 0.022 | 0.052 | 52 | 2.625 | 0.036 | 0.010 | 0.002 |
| 22 | 1.125 | 2.087 | 0.019 | 0.020 | 53 | 2.675 | 0.050 | 0.014 | 0.005 |
| 23 | 1.175 | 1.847 | 0.018 | 0.056 | 54 | 2.725 | 0.066 | 0.018 | 0.010 |
| 24 | 1.225 | 1.667 | 0.017 | 0.050 | 55 | 2.775 | 0.083 | 0.021 | 0.013 |
| 25 | 1.275 | 1.486 | 0.016 | 0.015 | 56 | 2.825 | 0.102 | 0.050 | 0.019 |
| 26 | 1.325 | 1.339 | 0.015 | 0.039 | 57 | 2.875 | 0.132 | 0.079 | 0.034 |
| 27 | 1.375 | 1.229 | 0.015 | 0.022 | 58 | 2.925 | 0.165 | 0.113 | 0.040 |
| 28 | 1.425 | 1.132 | 0.014 | 0.031 | 59 | 2.975 | 0.178 | 0.079 | 0.043 |
| 29 | 1.475 | 1.025 | 0.014 | 0.032 | 60 | 3.025 | 0.165 | 0.073 | 0.041 |
| 30 | 1.525 | 0.913 | 0.013 | 0.027 | 61 | 3.075 | 0.203 | 0.098 | 0.056 |
| 31 | 1.575 | 0.818 | 0.013 | 0.014 | 62 | 3.125 | 0.287 | 0.138 | 0.081 |

$$h(s) \;=\; \frac{2}{\pi}\frac{k(s)}{\sqrt{s}}\ln\left(\frac{\sqrt{s}+2k(s)}{2m_\pi}\right)\,, \tag{15}$$

with $dh/ds|_{M_i^2} = h(M_i^2)\left[(8k^2(M_i^2))^{-1} - (2M_i^2)^{-1}\right] + (2\pi M_i^2)^{-1}$ and

$$d = \frac{3}{\pi}\frac{m_\pi^2}{k^2(M_i^2)}\ln\left(\frac{M_i+2k(M_i^2)}{2m_\pi}\right) + \frac{M_i}{2\pi k(M_i^2)} - \frac{m_\pi^2 M_i}{\pi k^3(M_i^2)}\,. \tag{16}$$

Note that the function $d$ is chosen so that the $BW^{GS}$ function is unity at $s = 0$ [50].

Since the unfolded mass spectrum has bin-by-bin correlations, the off-diagonal components of the covariance matrix $X$ are included in the $\chi^2$ evaluation:

$$\chi^2 = \sum_{i,j}\left(y_i - f(s_i;\alpha)\right)(X^{-1})_{ij}\left(y_j - f(s_j;\alpha)\right)\,, \tag{17}$$

where $y_i$ is the measured value at the $i$-th bin, $f(s;\alpha)$ is the value of the function for parameters $\alpha$, and $(X^{-1})_{ij}$ is the inverse of the covariance matrix.

There are 10 parameters in this formula: the masses ($M_i$) and widths ($\Gamma_i$) for the $\rho$, $\rho'$, and $\rho''$ resonances, their relative amplitudes $|\beta|, |\gamma|$, and phases $\phi_\beta$ and $\phi_\gamma$. In addition, as an overall normalization factor, we introduce $|F_\pi(0)|^2$ as an additional parameter. In the BW form, this value should be unity. However, in order to take into account a possible deviation from the form of the fitting function, two kinds of fits, in which this parameter is either fixed or floated, are carried out. The other 10 parameters are floated in the fit.

The results of the fit are shown as the solid line in Fig. 9 for the $M^2_{\pi\pi^0}$ distribution as well as in Fig. 10 and Fig. 11(a) and (b), where the results are compared directly to the weak form factor squared $|F_\pi^-(s)|^2$, derived bin-by-bin from Eq. (7). In Eq. (7), we use the world average value (including our measurement) for the branching fraction $\mathcal{B}_{\pi\pi} = (25.24 \pm 0.10)\%$ and for the CKM matrix element $V_{ud} = 0.97377 \pm 0.00027$ [31]. For the short-distance radiative correction $S_{\rm EW} = S^{\pi\pi}_{\rm EW}/S^{e}_{\rm EW}$, we take the value $1.0235 \pm 0.0003$, to be consistent with the isospin breaking correction discussed in Ref. [5, 30] (see the appendix for more details).

The fitted results are summarized in Table VII for the cases when $|F_\pi(0)|^2$ is fixed to unity (the second column) and is allowed to float (the third column). In the table, the first error is statistical and the second is systematic. The value of the $\chi^2$ per degree of freedom (NDF) is 80/52 for the fixed and 65/51 for the floated cases. It is found that $|F_\pi(0)|^2$ is close to unity ($|F_\pi(0)|^2 = 1.02 \pm 0.01 \pm 0.04$) even when it is allowed to float. It should be noted that the data can be fitted using BW resonances only, without any additional background terms. The fit quality for the fixed case is slightly worse than that for the floated one. The curves shown in Figs. 9, 10 and 11(a) and 11(b), correspond to the case when the parameter $|F_\pi(0)|^2$ is floated, but the differences between the floated and the fixed cases are small.

The significance of the $\rho''(1700)$ signal is given in the last row of Table VII. The significance is determined from the change in the $\chi^2$ when the signal and its associated degree of freedom are removed from the fit. If the $\rho''(1700)$ signal is excluded from the fit, the $\chi^2$ for the fit increases by 55 (60) units, in the case that $|F(0)|^2$ is fixed to unity (allowed to float). This increase in the $\chi^2$ for the fit, with the joint estimation of four removed parameters (mass, width, $|\gamma|$, $\phi_\gamma$), corresponds to a $6.5\sigma$ ($7.0\sigma$) significance for the $\rho''(1700)$ signal [51].

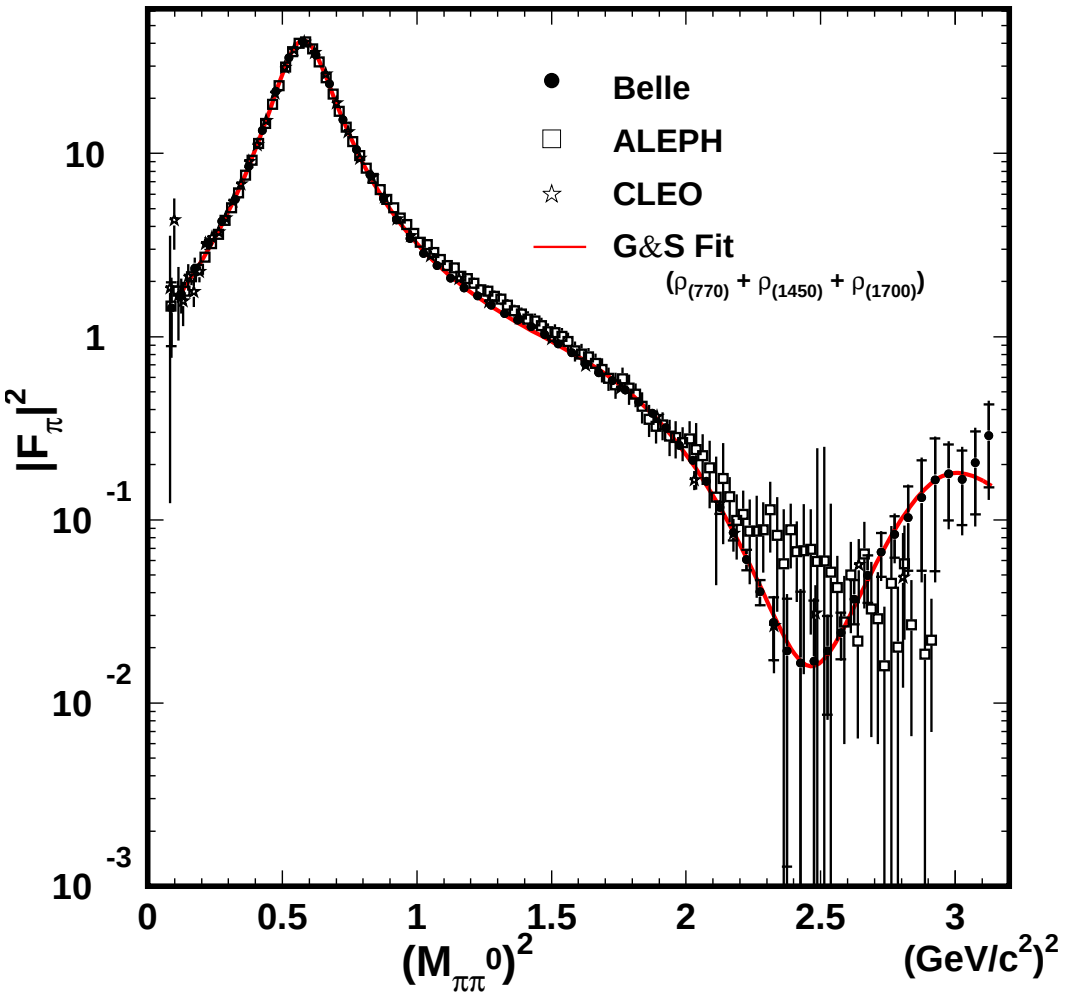


FIG. 10: Pion form factor for $\tau^- \to \pi^- \pi^0 \nu_\tau$. The solid circles are the Belle result while the squares and stars show the result of ALEPH [19] and CLEO [20], respectively. The error bars for the Belle data include both statistical and systematic errors added in quadrature. The solid curve is the result of a fit to the Gounaris-Sakurai model with the $\rho(770)$, $\rho'(1450)$, and $\rho''(1700)$ resonances, where all parameters are floated.

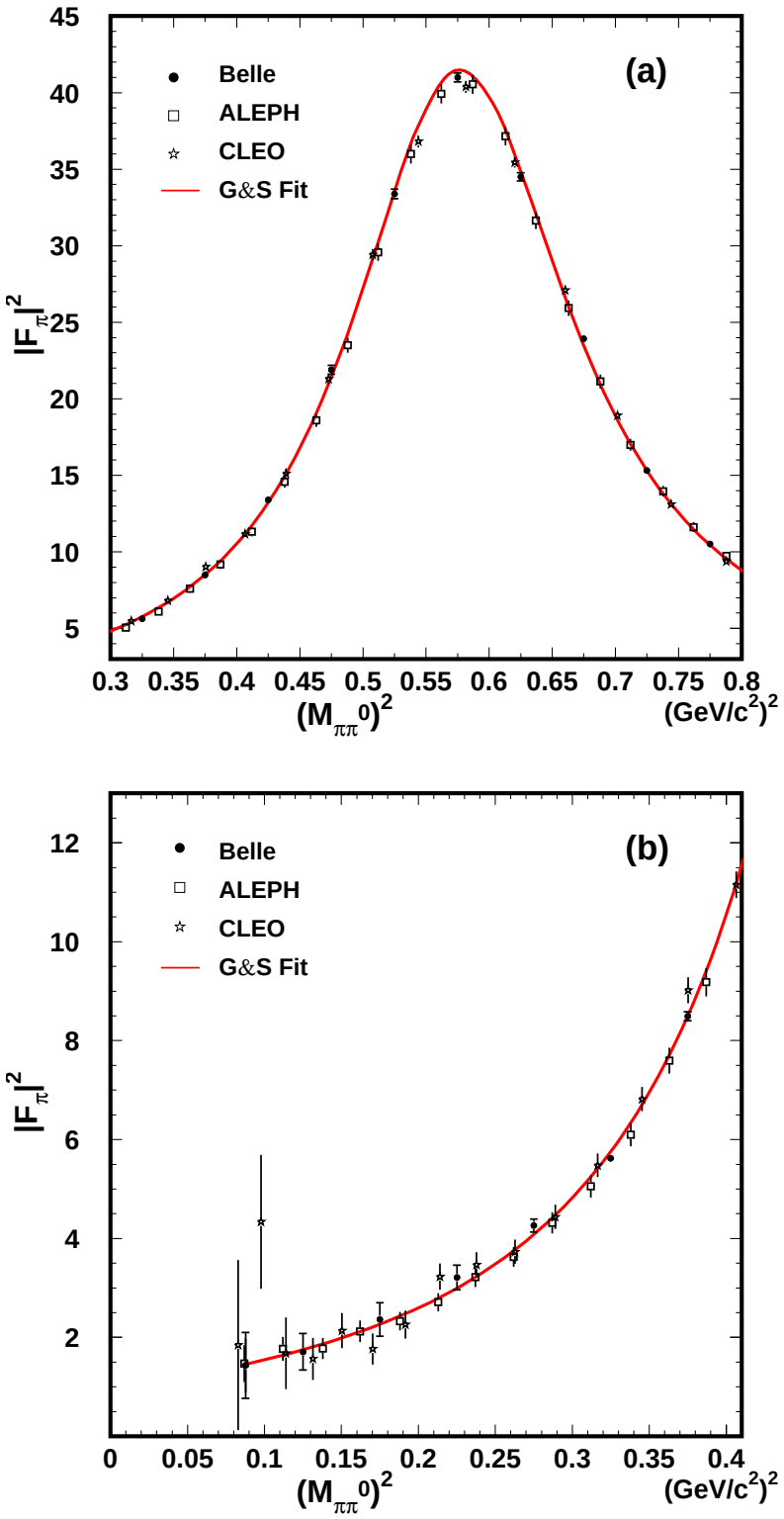


FIG. 11: (a) Pion form factor for $\tau^- \to \pi^- \pi^0 \nu_\tau$ in the $\rho(770)$ mass region and (b) in the threshold region. The convention of the plots is the same as in Fig. 10. The error bars for the Belle data include both statistical and systematic errors added in quadrature. The solid curve is the result of a fit to the Gounaris-Sakurai model, where all parameters are floated. See the text for details.

TABLE VII: Results of fitting the $M^2_{\pi\pi^0}$ distribution for $\tau^- \to \pi^-\pi^0\,\nu_\tau$ to the Gounaris-Sakurai model with the $\rho(770)$, $\rho'(1450)$, and $\rho''(1700)$ resonances. The results are shown for two cases, fixed $|F_\pi(0)|^2 = 1$ (the second column) and all parameters are allowed to float (the third column). The first error is statistical and the second one is systematic. The systematic errors include the uncertainty in the backgrounds, unfolding as well as the uncertainty of the photon energy scale. The last row gives the significance of the $\rho''(1700)$ signal.

| Parameter | Fit result (fixed $\lvert F(0)\rvert^2$) | Fit result (all free) |
|---|---|---|
| $M_\rho$, MeV/$c^2$ | $774.6 \pm 0.2 \pm 0.5$ | $774.9 \pm 0.3 \pm 0.5$ |
| $\Gamma_\rho$, MeV | $148.1 \pm 0.4 \pm 1.7$ | $148.6 \pm 0.5 \pm 1.7$ |
| $M_{\rho'}$, MeV/$c^2$ | $1446 \pm 7 \pm 28$ | $1428 \pm 15 \pm 26$ |
| $\Gamma_{\rho'}$, MeV | $434 \pm 16 \pm 60$ | $413 \pm 12 \pm 57$ |
| $\lvert\beta\rvert$ | $0.15 \pm 0.05^{+0.15}_{-0.04}$ | $0.13 \pm 0.01^{+0.16}_{-0.04}$ |
| $\phi_\beta$, degree | $202 \pm 4^{+41}_{-\ 8}$ | $197 \pm 9^{+50}_{-\ 5}$ |
| $M_{\rho''}$, MeV/$c^2$ | $1728 \pm 17 \pm 89$ | $1694 \pm 41 \pm 89$ |
| $\Gamma_{\rho''}$, MeV | $164 \pm 21^{+89}_{-26}$ | $135 \pm 36^{+50}_{-26}$ |
| $\lvert\gamma\rvert$ | $0.037 \pm 0.006^{+0.065}_{-0.009}$ | $0.028 \pm 0.020^{+0.059}_{-0.009}$ |
| $\phi_\gamma$, degree | $24 \pm 9^{+118}_{-\ 28}$ | $-3 \pm 13^{+136}_{-\ 29}$ |
| $\lvert F(0)\rvert^2$ | [1.0] | $1.02 \pm 0.01 \pm 0.04$ |
| $\chi^2$/NDF | 80/52 | 65/51 |
| $\rho''(1700)$ signif., $\sigma$ | 6.5 | 7.0 |

The fit parameters are correlated, with the correlation matrix:

$$\begin{pmatrix}
1.00 & & & & & & & & & & \\
0.58 & 1.00 & & & & & & & & & \\
0.45 & 0.39 & 1.00 & & & & & & & & \\
-0.30 & -0.13 & 0.24 & 1.00 & & & & & & & \\
-0.14 & -0.28 & -0.15 & 0.36 & 1.00 & & & & & & \\
-0.31 & -0.24 & -0.06 & 0.47 & 0.13 & 1.00 & & & & & \\
-0.42 & -0.08 & 0.25 & 0.34 & -0.61 & 0.38 & 1.00 & & & & \\
0.31 & 0.22 & 0.08 & -0.10 & -0.41 & 0.37 & 0.29 & 1.00 & & & \\
0.32 & 0.27 & 0.13 & -0.13 & -0.44 & 0.48 & 0.28 & 0.64 & 1.00 & & \\
0.54. & 0.29 & -0.01 & -0.07 & 0.05 & 0.52 & -0.27 & 0.54 & 0.67 & 1.00 & \\
-0.19 & -0.06 & 0.13 & 0.61 & 0.23 & 0.49 & 0.57 & 0.53 & 0.17 & 0.07 & 1.00
\end{pmatrix}, \qquad (18)$$

where the parameters are $|F_\pi(0)|^2$, $M_\rho$, $\Gamma_\rho$, $M_{\rho'}$, $\Gamma_{\rho'}$, $|\beta|$, $\phi_\beta$, $M_{\rho''}$, $\Gamma_{\rho''}$, $|\gamma|$ and $\phi_\gamma$.

The systematic uncertainties for the parameters are summarized in Table VIII, where the sources of the systematic errors from the unfolding procedure (UNF), the $q\bar{q}$ background subtraction (BKG1), the feed-down background subtraction (BKG2), the acceptance correction (ACC) and the photon energy scale (PES) are shown separately. The uncertainty in the $\rho$ mass (0.7 MeV/$c^2$) is mainly due to the uncertainty in the photon energy scale.

TABLE VIII: Systematic errors for resonance parameters from the unfolding procedure (UNF), the background subtraction (BKG), the acceptance correction (ACC) and the photon energy scale (PES).

| | $M_\rho$ (MeV/$c^2$) | $\Gamma_\rho$ (MeV) | $M_{\rho'}$ (MeV/$c^2$) | $\Gamma_{\rho'}$ (MeV) | $\lvert\beta\rvert$ | $\phi_\beta$ (deg.) | $M_{\rho''}$ (MeV/$c^2$) | $\Gamma_{\rho''}$ (MeV) | $\lvert\gamma\rvert$ | $\phi_\gamma$ (deg.) |
|---|---|---|---|---|---|---|---|---|---|---|
| Fit Bias | 0.3 | 1.6 | 25 | 49 | 0.028 | 4 | 75 | 10 | 0.006 | 13 |
| UNF | 0.3 | 0.3 | 4 | 24 | 0.020 | 4 | 11 | 14 | 0.002 | 12 |
| BKG1 | 0.3 | ... | 11 | 25 | $^{+0.143}_{-0.031}$ | $^{+41}_{-5}$ | 13 | $^{+86}_{-10}$ | $^{+0.053}_{-0.020}$ | $^{+117}_{-22}$ |
| BKG2 | ... | ... | 1 | ... | ... | 2 | 2 | 2 | 0.001 | ... |
| ACC | ... | 0.1 | 1 | 4 | ... | ... | ... | 7 | ... | 1 |
| PES | 0.3 | 0.6 | 2 | 1 | ... | 2 | 45 | 15 | ... | 1 |
| Total | 0.5 | 1.7 | 28 | 60 | $^{+0.147}_{-0.047}$ | $^{+41}_{-8}$ | 89 | $^{+89}_{-26}$ | $^{+0.053}_{-0.021}$ | $^{+118}_{-28}$ |

The uncertainty in the $q\bar{q}$ background (BKG1) dominates for the $\rho'(1450)$ and $\rho''(1700)$ resonance parameters.

The values of the $\rho(770)$ mass and width are consistent with the results of the previous measurements in $\tau$ decay. For the $\rho'(1450)$, a slightly higher mass value than in the previous measurement is obtained. It is found that this value is sensitive to the value of the resonance parameters for the $\rho''(1700)$ since they both interfere. This is the first time that all the parameters for the $\rho(770)$, $\rho'(1450)$ and $\rho''(1700)$ are determined in a single fit. Production of the $\rho''(1700)$ in $\tau^-$ decays has been unambiguously demonstrated and its parameters determined.

### E. Comparison of Belle and previous $\tau$ data

Comparisons of the pion form factor squared $|F_\pi^-(s)|^2$ measured in Belle to those measured by CLEO [20] and ALEPH [19] experiments are given in Fig. 11(a) for the $\rho(770)$ region and in Fig. 11(b) for the low-mass region $M^2_{\pi\pi^0} < 0.4(\mathrm{GeV}/c^2)^2$. Figure 12 shows a more detailed comparison, the difference in $|F_\pi(s)|^2$ of Belle and CLEO, ALEPH data for the fit of the Belle data divided by the fit value, for the mass-squared range 0.11–1.20 $(\mathrm{GeV}/c^2)^2$. It can be seen that over the entire mass range shown, the $|F_\pi(s)|^2$ values from Belle are consistent within errors with those of CLEO. Agreement is worse when Belle data are compared to ALEPH data. Below 0.5 $(\mathrm{GeV}/c^2)^2$ our points are mostly higher than those of ALEPH, while above 0.7 $(\mathrm{GeV}/c^2)^2$ they are systematically and significantly lower.

## VI. IMPLICATIONS FOR THE MUON ANOMALOUS MAGNETIC MOMENT

### A. Basic Formula

As described in the introduction, the hadronic vacuum polarization term $a_\mu^{\mathrm{had,LO}}$ plays an important role in the standard model prediction for the muon anomalous magnetic moment $a_\mu$; the error on this contribution is the most significant source of the uncertainty in $a_\mu$. In this section, we discuss the implication of our measurement for the determination of $a_\mu^{\mathrm{had.LO}}$.

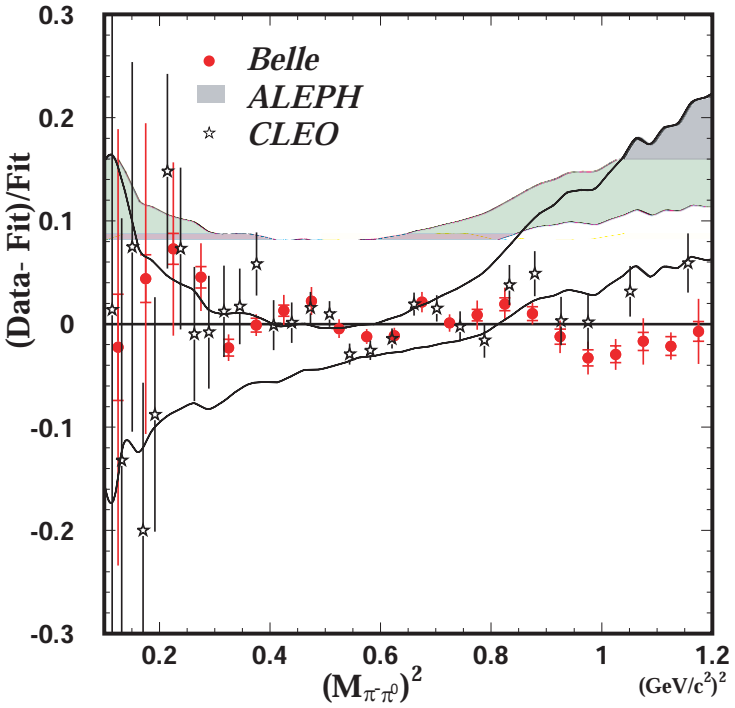


FIG. 12: Comparison of the pion form factor squared $|F_\pi(s)|^2$ measured with the Belle detector to results from the CLEO [20] and ALEPH [19] experiments in the $\rho(770)$ and $\rho'(1450)$ mass region. The difference from the fit of the Belle $\tau^-\to\pi^-\pi^0\,\nu_\tau$ data divided by the fit value is plotted. The solid circles show the Belle result, the open stars show the CLEO result [20] and the hatched band shows the ALEPH result [19]. Both Belle and ALEPH results include the systematic errors. The inner error bars in the Belle data indicate the statistical errors.

The value of $a_\mu^{\rm had,LO}$ is related to the $e^+e^-$ annihilation cross section via the dispersion integral

$$a_\mu^{\rm had,LO} = \frac{1}{4\pi^3}\int_{4m_\pi^2}^{\infty}\sigma^0_{\rm had}(s)\left(\frac{m_\mu^2}{3s}\right)\hat{K}(s)\,{\rm d}s\,, \tag{19}$$

where $\sigma^0_{\rm had}$ is the total cross section for $e^+e^-\to$hadrons at the center-of-mass energy $\sqrt{s}$. The superscript in $\sigma^0_{\rm had}$ denotes the "bare" hadronic cross section, which is defined as the measured cross section, corrected for QED radiative corrections such as initial state radiation, electron-vertex correction and the vacuum polarization in the photon propagator. However, the final state radiation (FSR) photons coming from the process $\sigma^0(e^+e^-\to V\gamma\to\pi^+\pi^-\gamma)$ should be included in the $\sigma^0_{\rm had}$ term (See the detailed discussion on page 12 of Ref. [5]). The kernel function $\hat{K}(s)$ is given by

$$\begin{aligned}\hat{K}(s) \;=\; & \frac{3s}{m_\mu^2}\left\{x^2\left(1-\frac{x^2}{2}\right)+(1+x)^2\left(1+\frac{1}{x^2}\right)\left(\ln(1+x)\right.\right.\\ & -\;\left.\left. x+\frac{x^2}{2}\right)+\left(\frac{1+x}{1-x}\right)x^2\ln x\right\}.\end{aligned}$$

with $x = (1-\beta_\mu)/(1+\beta_\mu)$ and $\beta_\mu \equiv \sqrt{1-4m_\mu^2/s}$. $\hat{K}(s)$ is a smooth function increasing from 0.63 at the threshold $s = 4m_\pi^2$ to unity at $s = \infty$. Because of the $1/s$ dependence of $\sigma^0_{\rm had}(s)$ and the additional $1/s$ factor in the integral in Eq. (19), low-mass hadronic final states dominate the contribution to $a_\mu^{\rm had,LO}$; in fact about 70% of $a_\mu^{\rm had,LO}$ is due to the two-pion final state with $4m_\pi^2 \le s \le 0.8$ (GeV/$c^2$)$^2$. Consequently, the $2\pi$ mass spectrum from $\tau$ data is useful for obtaining predictions for $a_\mu^{\rm had,LO}$ using CVC.

TABLE IX: Summary of the $a_\mu^{\pi\pi}$ contribution from $\tau$ data from Belle, ALEPH [19] and CLEO [20] experiments. The errors are only shown for the Belle data. In this table, the isospin breaking correction is not applied except for the short-distance radiative correction given by the term $S_{\rm EW}$. The errors in the Belle data are only statistical. The errors for other experiments are similar or slightly worse than the Belle value in the same mass range.

| $M^2_{\pi\pi^0}$ range | $a_\mu^{\pi\pi}$ ($10^{-10}$) | | | Integrated $a_\mu^{\pi\pi}$ ($10^{-10}$) | | |
|---|---|---|---|---|---|---|
| ((GeV/$c^2$)$^2$) | Belle | ALEPH | CLEO$^{(*)}$ | Belle | ALEPH | CLEO$^{(*)}$ |
| 0.075-0.200 | 39.55 ± 0.97 | 38.20 | 43.81 | 39.55 ± 0.97 | 38.20 | 43.81 |
| 0.200-0.350 | 70.62 ± 0.46 | 66.84 | 75.71 | 110.3 ± 1.07 | 105.0 | 119.5 |
| 0.350-0.500 | 123.25 ± 0.28 | 119.10 | 106.10 | 233.5 ± 1.11 | 224.1 | 225.6 |
| 0.500-0.650 | 196.78 ± 0.23 | 194.00 | 197.80 | 430.3 ± 1.13 | 418.2 | 423.3 |
| 0.650-0.800 | 62.35 ± 0.10 | 62.35 | 73.03 | 492.6 ± 1.14 | 480.5 | 496.3 |
| 0.800-0.950 | 15.64 ± 0.04 | 16.40 | 14.31 | 508.3 ± 1.14 | 496.9 | 510.6 |
| 0.950-1.100 | 5.74 ± 0.02 | 6.50 | 6.01 | 514.0 ± 1.14 | 503.4 | 516.6 |
| 1.100-1.250 | 2.86 ± 0.01 | 3.27 | 2.32 | 516.9 ± 1.14 | 506.7 | 519.0 |
| 1.250-1.400 | 1.65 ± 0.01 | 1.89 | 2.65 | 518.5 ± 1.14 | 508.6 | 521.6 |
| 1.400-1.550 | 1.03 ± 0.01 | 1.13 | 0.77 | 519.5 ± 1.14 | 509.7 | 522.4 |
| 1.550-1.700 | 0.60 ± 0.00 | 0.66 | 0.49 | 520.2 ± 1.14 | 510.3 | 522.9 |
| 1.700-1.850 | 0.36 ± 0.00 | 0.37 | 0.33 | 520.5 ± 1.14 | 510.7 | 523.2 |
| 1.850-2.000 | 0.19 ± 0.00 | 0.19 | 0.21 | 520.7 ± 1.14 | 510.9 | 523.4 |
| 2.000-2.600 | 0.13 ± 0.00 | 0.21 | 0.15 | 521,8 ± 1.14 | 511.1 | 523.6 |
| 2.600-3.200 | 0.13 ± 0.00 | 0.21 | 0.04 | 522.0 ± 1.14 | 511.1 | 523.6 |

$^{(*)}$ For the CLEO data, the boundary of the mass range is slightly different from the one shown in the first column, since $\sqrt{s}$ bins are used.

### B. Results

Details of our determination of $a_\mu^{\pi\pi}$, the $2\pi$ contribution to $a_\mu^{\rm had,LO}$, are given in the appendix, where the basic formulas, the corrections applied for the isospin-violating effects, and discussions on the error estimation are presented.

Our result on $a_\mu^{\pi\pi}$ over the mass range $\sqrt{s} = 2m_\pi - 1.8$ GeV/$c^2$ is

$$a_\mu^{\pi\pi}[2m_\pi, 1.8\ {\rm GeV}/c^2] = (523.5 \pm 1.5\,({\rm exp.}) \pm 2.6\,({\rm Br.}) \pm 2.5\,({\rm isospin})) \times 10^{-10},$$

where the first error is due to the experimental uncertainties, *i.e.* the statistical error ($1.1 \times 10^{-10}$) and experimental systematic error ($1.0 \times 10^{-10}$) added in quadrature. The second error comes from the uncertainties in the branching fractions. The third one is the error on the isospin-violating corrections. These sources of error are discussed in the appendix.

This result can be compared to those from previous ALEPH, CLEO, and OPAL $\tau$ data. The combined result given in Ref. [5] is

$$a_\mu^{\pi\pi}[2m_\pi, 1.80\ \mathrm{GeV}/c^2] = (520.1 \pm 2.4\,(\mathrm{exp.}) \pm 2.7(\mathrm{Br.}) \pm 2.5\,(\mathrm{isospin})) \times 10^{-10} \quad (\tau)\,.$$

In terms of the experimental error (i.e. the first uncertainty), our result improves the previous combined result by 40%. A detailed comparison from our results and those of ALEPH [19] and CLEO [20] is given in Table IX for the $a_\mu^{\pi\pi}$ contribution. As seen in Table IX, the contribution from the mass-squared region $0.8\ (\mathrm{GeV}/c^2)^2 < s < 1.25\ (\mathrm{GeV}/c^2)^2$, where one observes a deviation between the Belle and ALEPH data in Fig. 9, is only 4.6% of the total $2\pi$ contribution. In this region, the contribution from the ALEPH measurements is higher than that from Belle but it is compensated by the opposite tendency in the region $s < 0.50\ (\mathrm{GeV}/c^2)^2$. Moreover, since the contribution from CLEO is between Belle and ALEPH, the difference between our result and the combined previous-$\tau$ result becomes smaller. Consequently, our result agrees well with that of the combined result given from the previous $\tau$ data within $< 1\sigma$ of the experimental error.

On the other hand, the value of $a_\mu^{\pi\pi}$ in the same $\sqrt{s}$ region evaluated from the $e^+e^-$ cross section measurements is [27]

$$a_\mu^{\pi\pi}[2m_\pi, 1.80\ \mathrm{GeV}/c^2] = (504.6 \pm 3.1\,(\mathrm{exp.}) \pm 0.9\,(\mathrm{rad.})) \times 10^{-10} \qquad (e^+e^-:\mathrm{CMD2,SND})\,,$$

where the first error includes both statistical and experimental systematic errors added in quadrature. The second error is due to radiative corrections.

Our $\tau$ result is noticeably higher than the $e^+e^-$ result. This confirms the longstanding difference between the spectral functions of the $2\pi$ systems produced in $\tau$-decay and $e^+e^-$ annihilation [52].

In summary, we have studied the decay $\tau^- \to \pi^-\pi^0\,\nu_\tau$ using a high-statistics data sample taken with the Belle detector at the KEKB $e^+e^-$ collider. The branching fraction is measured with 1.5% accuracy. From Table III we can calculate the accuracy of the previous experiments: CLEO 1.7%, L3 2.4%, OPAL 1.3%, ALEPH 0.5%, DELPHI 0.9%. These comparison shows that the accuracy of the Belle result is better than CLEO and L3, similar to OPAL and worse than ALEPH and DELPHI. The result is in good agreement with previous measurements. In the unfolded $\pi^-\pi^0$ mass spectrum, in addition to the $\rho(770)$ and $\rho'(1450)$ mesons, the production of the $\rho''(1700)$ in $\tau^-$ decays has been unambiguously demonstrated and its parameters determined. The unfolded spectrum is used to evaluate the $2\pi$ contribution to the muon anomalous magnetic moment $a_\mu^{\pi\pi}$ in the region $\sqrt{s} = 2m_\pi - 1.80\ \mathrm{GeV}/c^2$. Our results agree well with the previous $\tau$ based results but are higher than those from $e^+e^-$ annihilation.

**Acknowledgments**

We thank M. Davier and J. H. Kühn for their advice and encouragement during this analysis. We thank S. Dubnička for a useful discussion about the BW resonance form.

We are grateful to G. López Castro for providing the table of the long-distance radiative corrections for $\tau^- \to \pi^-\pi^0\,\nu_\tau$. We thank the KEKB group for the excellent operation of the accelerator, the KEK cryogenics group for the efficient operation of the solenoid, and the KEK computer group and the National Institute of Informatics for valuable computing and SINET3 network support. We acknowledge support from the Ministry of Education, Culture, Sports, Science, and Technology of Japan and the Japan Society for the Promotion of Science; the Australian Research Council and the Australian Department of Education, Science and Training; the National Natural Science Foundation of China under Contracts No. 10575109 and No. 10775142; the Department of Science and Technology of India; the BK21 program of the Ministry of Education of Korea, the CHEP SRC program and Basic Research program (Grant No. R01-2005-000-10089-0) of the Korea Science and Engineering Foundation, and the Pure Basic Research Group program of the Korea Research Foundation; the Polish State Committee for Scientific Research; the Ministry of Education and Science of the Russian Federation and the Russian Federal Agency for Atomic Energy; the Slovenian Research Agency; the Swiss National Science Foundation; the National Science Council and the Ministry of Education of Taiwan; and the U.S. Department of Energy.

## Appendix

### C. Determination of $a_\mu^{\pi\pi}$ from Belle data

In this appendix, we list the details of our determination of $a_\mu^{\pi\pi}$ over the range $\sqrt{s} = 2m_\pi - 1.8$ GeV/$c^2$. We discuss the basic formula, the integration procedure, the corrections for the isospin-violating effects, and the evaluation of the experimental errors.

#### *1. Basic formula*

In the isospin symmetry limit, CVC relates the quantities in $\tau^- \to \pi^-\pi^0\,\nu_\tau$ decay to the cross section $e^+e^- \to \pi^+\pi^-$ ($\sigma^0_{\pi\pi}$) through the relation [30]

$$\begin{aligned}\sigma^0_{\pi\pi}|_{\rm CVC} &= \frac{1}{\mathcal{N}(s)\Gamma^0_e}\frac{{\rm d}\Gamma(\tau^-\to\pi^-\pi^0\,\nu_\tau)}{{\rm d}s} \\ &= \frac{1}{\mathcal{N}(s)} \times \left(\frac{\mathcal{B}_{\pi\pi}}{B_e}\right) \times \left(\frac{1}{N_{\pi\pi}}\frac{{\rm d}N_{\pi\pi}}{{\rm d}s}\right), \end{aligned} \tag{20}$$

where $\mathcal{N}(s)$ is given by

$$\mathcal{N}(s) = \frac{3|V_{ud}|^2}{2\pi\alpha_0^2 m_\tau^2} s \left(1 - \frac{s}{m_\tau^2}\right)^2 \left(1 + \frac{2s}{m_\tau^2}\right). \tag{21}$$

A more precise link between hadronic spectral functions from $\tau$ decays and the $e^+e^-$ hadronic cross section requires a calculation of radiative corrections as well as the inclusion of the isospin breaking effects (both of kinematic and dynamic origin). These effects have recently been discussed by Cirigliano *et al.* [30] and by Flores-Tlalpa *et al.* [53]. According to them, the formula in Eq. (20) is modified to

$$\sigma^0_{\pi^+\pi^-}|_{\rm CVC} = \frac{1}{\mathcal{N}(s)} \times \left(\frac{\mathcal{B}_{\pi\pi}}{B_e}\right) \times \left(\frac{1}{N_{\pi\pi}}\frac{{\rm d}N_{\pi\pi}}{{\rm d}s}\right) \left(\frac{R_{\rm IB}(s)}{S_{\rm EW}}\right), \tag{22}$$

with

$$R_{\rm IB}(s) = \frac{1}{G_{\rm EM}(s)}\frac{\beta_0^3(s)}{\beta_-(s)}\left|\frac{F_0(s)}{F_-(s)}\right|^2, \tag{23}$$

where $S_{\rm EW}$ is the dominant short-distance electroweak correction and $R_{\rm IB}(s)$ takes care of the isospin-violating corrections. $R_{\rm IB}(s)$ includes the long-distance QED correction $G_{\rm EM}(s)$, the phase space correction factor $\beta_0^3(s)/\beta_-^3(s)$, and the ratio of the pion form factors $|F_0(s)/F_-(s)|^2$.

#### *2. Integration procedure*

Using the measured distribution $(1/N_{\pi\pi})({\rm d}N_{\pi\pi}/{\rm d}s)$, the moment $a_\mu^{\pi\pi}$ can be obtained by inserting the bare cross section Eq. (22) to Eq. (19) and integrating over $s$. The integration in Eq. (19) is carried out numerically by taking the sum of the integrand evaluated at

the center of each bin. The statistical error on $a_\mu^{\pi\pi}$ is calculated including the off-diagonal elements of the covariance error matrix $X_{ij}$:

$$\Delta a_\mu^{\pi\pi} = \sum_{i,j} \left(\frac{\partial a_\mu}{\partial \alpha_i}\right) X_{ij} \left(\frac{\partial a_\mu}{\partial \alpha_j}\right). \tag{24}$$

There are several external parameters in these equations; the values used for them are listed in Table X. For $m_\tau$, $V_{ud}$, and $\mathcal{B}_e$, PDG [31] values are used. For the $\pi^-\pi^0$ branching fraction, our measurement is consistent with the world average given in Ref. [31]. Including our result and the recent ALEPH $\mathcal{B}_{\pi\pi^0}$ measurement [19], the new world average is

$$\mathcal{B}_{\pi\pi^0} = (25.42 \pm 0.10)\%. \tag{25}$$

We use this new world average for the evaluation of $a_\mu^{\pi\pi}$.

The errors on $a_\mu^{\pi\pi}$ arising from external parameters are summarized in Table X; the total systematic error from these sources is $\pm 2.7 \times 10^{-10}$ (dominated by $\Delta\mathcal{B}_{\pi\pi^0}$).

TABLE X: Values of the external parameters and systematic errors on $a_\mu^{\pi\pi}$ arising from these sources.

| Source | Value | Relative error (%) | $\Delta a_\mu^{\pi\pi}$ ($10^{-10}$) | Reference |
|---|---|---|---|---|
| $V_{ud}$ | $0.97377 \pm 0.00027$ | 0.027 | $\pm$ 0.26 | [31] |
| $\mathcal{B}_e$ | $(17.84 \pm 0.05)\%$ | 0.28 | $\pm$ 1.45 | [31] |
| $\mathcal{B}_{\pi\pi^0}$ | $(25.42 \pm 0.10)\%$ | 0.41 | $\pm$ 2.13 | |
| Total external | | | $\pm$ 2.6 | |

*3. Experimental systematic uncertainty*

The systematic errors on $a_\mu^{\pi\pi}$ arising from internal sources (specific to this measurement) are listed in Table XI and discussed below. There are two sources of background in the $\pi^-\pi^0$ sample: (i) feed-down from $\tau^- \to h^-(n\pi^0)\nu_\tau$, $\tau^- \to K^-\pi^0\nu_\tau$, $\tau^- \to \omega\pi^-\nu_\tau(\omega \to \pi^0\gamma)$ and (ii) non-$\tau$ background. In the first case, MC statistics and the uncertainty on the branching fraction are used to estimate the error. In the second case, the uncertainty on the background as estimated from the control samples is assigned as an error. As mentioned earlier, the fake-$\pi^0$ background is subtracted using sideband events and the uncertainty is determined by varying the signal and sideband regions.

It is found that the shape of the mass spectrum is insensitive to uncertainties in the $\pi^0$ efficiency, as it is only at a few % level. The uncertainty of the integration procedure comes from the binning effects. Adding all individual errors in quadrature we obtain a total error on $a_\mu^{\pi\pi}$ arising from internal sources of $\pm 1.0 \times 10^{-10}$.

To check the stability of $a_\mu^{\pi\pi}$, we perform the following tests:

1. The sample is divided into subsamples based on the tag-side topology, i.e., one electron, one-prong, or three-prong. The values of $a_\mu^{\pi\pi}$ obtained from these subsamples are consistent within the statistical errors.

TABLE XI: Systematic errors on $a_\mu^{\pi\pi}$ arising from internal sources (specific to this measurement).

| Source | $\Delta a_\mu^{\pi\pi} \times 10^{10}$ |
|---|---|
| Background: | |
| non-$\tau$ ($e^+e^- \to \bar{q}q$) | $\pm$ 0.11 |
| feed-down $h(n\pi^0)\nu$ | $\pm$ 0.09 |
| feed-down $K^-\pi^0\nu$ | $\pm$ 0.15 |
| Energy scale | $\pm$ 0.10 |
| $\pi^0/\gamma$ selection | $\pm$ 0.24 |
| $\gamma$ veto | $\pm$ 0.93 |
| Efficiency: | |
| $\pi^0/\gamma$ | $\pm$ 0.35 |
| charged track | $< 0.10$ |
| Integration procedure | $< 0.10$ |
| Total internal | $\pm$ 1.04 |

2. The sample is divided into subsamples based on the running period. Again, the values of $a_\mu^{\pi\pi}$ obtained are consistent within the statistical errors.

3. The sample might be sensitive to the requirement on the overlap region between the charged track and $\gamma$ clusters. To estimate this sensitivity, we select events with a tighter isolation requirement on $\gamma$'s and on the track extrapolation: 30 cm instead of 20 cm.

   The resulting variation in $a_\mu^{\pi\pi}$ is small and is included as an additional systematic error.

*4. Isospin-violating corrections for $a_\mu^{\pi\pi}$*

Three identifiable sources of isospin breaking corrections are the mass difference of the charged and neutral pions, $\rho-\omega$ interference effects and the radiative corrections, which are included in the factor $R_{\rm IB}(s)/S_{\rm EW}$ in Eq. (20). The size of the isospin-violating corrections from these sources and the possible uncertainties from other sources are summarized in Table XII.

(i) The dominant contribution from electroweak radiative corrections comes from the short-distance corrections. In the leading logarithmic order, the short-distance radiative corrections to the decays $\tau^- \to (d\bar{u})\nu_\tau$ are enhanced by the factor [54], [55],

$$S(m_\tau, m_Z) = 1 + \frac{3\alpha(m_\tau)}{4\pi}(1 + 2\bar{Q}) \ln \frac{m_Z^2}{m_\tau^2} = 1.01878, \tag{26}$$

where $m_Z$ is the $Z$ boson mass, and $\alpha(m_\tau) = 1/133.50(2)$ is the QED coupling at the $\tau$ lepton mass. $\bar{Q}$ is the average quark-doublet charge. Therefore, $\bar{Q} = \frac{1}{2}(\frac{2}{3} - \frac{1}{3}) = \frac{1}{6}$

TABLE XII: Sources of the isospin violation between the $e^+e^-$ and $\tau$ spectral function in the $2\pi$ channel and the corrections to $a_\mu^{\pi\pi}$. The correction is based on the procedure given in Refs. [30, 53].

| Source of isospin violation | Correction to $a_\mu^{\pi\pi}$ $(10^{-10})$ | Uncertainty on $a_\mu^{\pi\pi}$ $(10^{-10})$ | References |
|---|---|---|---|
| Short-distance rad. cor. ($S_{\rm EW}$) | − 12.0 | ± 0.2 | [54], [55], [56], [5] |
| Long-distance rad. cor. ($G_{EM}(s)$) | − 1.0 | −− | [30], [53] |
| $m_{\pi^-} \neq m_{\pi^0}$ ($\beta^3$ in phase space) | − 7.0 | −− | |
| $\rho - \omega$ interference | + 3.5 | ± 0.6 | |
| $m_{\pi^-} \neq m_{\pi^0}$ ($\beta^3$ in the decay width) | + 4.2 | −− | |
| Electromagnetic decay modes | − 1.4 | ± 1.4 | |
| $m_{\rho^0} \neq m_{\rho^-}$ | −− | ± 2.0 | |
| Total | − 13.7 | ± 2.5 | |

for the semileptonic decays, $\tau \to \nu_\tau \bar{u}d$. Since $\bar{Q} = -\frac{1}{2}$ for leptons, there are no leading logarithmic corrections for leptonic decays.

We can go further and sum up all short-distance logarithms of the $\alpha^n \ln^n m_Z$ via the renormalization group. This procedure replaces Eq. (26) by

$$\begin{aligned} S(m_\tau, m_Z) \;=\; & \Big[\frac{\alpha(m_b)}{\alpha(m_\tau)}\Big]^{\frac{9}{19}} \Big[\frac{\alpha(m_W)}{\alpha(m_{m_b})}\Big]^{\frac{9}{20}} \Big[\frac{\alpha(m_Z)}{\alpha(m_W)}\Big]^{\frac{36}{17}} \\ & \Big[\frac{\alpha_s(m_b)}{\alpha_s(m_\tau)}\Big]^{\frac{3}{25}\frac{\alpha(m_\tau)}{\pi}} \Big[\frac{\alpha_s(m_Z)}{\alpha_s(m_b)}\Big]^{\frac{3}{23}\frac{\alpha(m_b)}{\pi}} = 1.01907\,, \end{aligned} \tag{27}$$

where the last two terms are the short-distance QCD corrections [56].

Taking into account the subleading correction for the leptonic decay, the short-distance Electroweak correction $S_{\rm EW}$ is given by

$$S_{\rm EW} = S(m_\tau, m_Z) \frac{1}{S_{\rm EW}^{e,sub}} = 1.0235 \pm 0.0003\,, \tag{28}$$

where $S_{\rm EW}^{e,sub} = \left(1 + \frac{\alpha(m_\tau)}{2\pi}\left(\frac{25}{4} - \pi^2\right)\right) = 0.9957$. The difference between the resummed value (1.01907) and the lowest-order estimate (1.01878) is taken as the error on $S_{\rm EW}$ and the resummed $S_{EW}$ value is used throughout this paper. The shift of $a_\mu^{\pi\pi}$ from this correction is $\triangle a_\mu^{\pi\pi} = (12.0 \pm 0.2) \times 10^{-10}$. Note that this correction is already applied in Eq. (7) and the pion form factor given in Table VI.

(ii) The long-distance QED radiative correction $G_{\rm EM}(s)$ was computed in the framework of chiral perturbation theory by Cirigliano *et al.* in Ref. [30] . Recently, it was reevaluated based on a meson dominance model by Flores-Tlalpa *et al.* in Ref. [53]. It is found that the predictions of both models coincide if the contribution of the $\omega(782)$ intermediate state $\tau \to \omega\pi^-\nu_\tau(\omega \to \pi^0\gamma)$, is excluded in the latter model calculation. Since in our data this intermediate $\omega(782)$ contribution is already subtracted at the analysis level, we use the $s$-dependent correction factor provided by Flores-Tlalpa, which does not include the $\omega$ contribution. This correction produces a shift of $\triangle a_\mu^{\pi\pi} = -1.0 \times 10^{-10}$,

(iii) The $\pi^-$ and $\pi^0$ mass difference in the ratio of the phase space $\beta_0^3/\beta_-^3$ results in a shift of $\triangle a_\mu^{\pi\pi} = -7.0 \times 10^{-10}$.

(iv) The $\pi^-$ and $\pi^0$ mass difference also affects the $\beta^3$ factor in the energy-dependent decay width (Eq. 13), which provides a positive shift $\triangle a_\mu^{\pi\pi} = +4.2 \times 10^{-10}$.

(v) The effect of the $\rho - \omega$ interference is estimated using the interference amplitude parameterized in the following form [30]:

$$F_\pi^0(s)_{\rho-\omega} = -\frac{\theta_{\rho\omega}}{3m_\rho^2} \frac{s}{m_\omega^2 - s - im_\omega\Gamma_\omega}\,. \tag{29}$$

For the numerical evaluation, we take $\theta_{\rho\omega} = (-3.3 \pm 0.7) \times 10^{-3}$ GeV$^2$, $m_\omega = 0.783$ GeV and $\Gamma_\omega = 0.00844$ GeV. The net effect is $\triangle a_\mu^{\pi\pi} = (+3.5 \pm 0.6) \times 10^{-10}$.

(vi) The largest source of the uncertainty for the isospin-violating effects is from the $\rho^-$ and $\rho^0$ mass difference. The mass difference is consistent with zero within about 1 MeV, which gives an uncertainty on $a_\mu^{\pi\pi}$ of $\pm 2.0 \times 10^{-10}$.

(vii) Finally, electromagnetic decay of the $\rho$ meson is the source of the isospin violation. The decay $\pi\pi\gamma$ deserves particular attention. The shift and its uncertainty are estimated to be $\triangle a_\mu^{\rm had} = (-1.4 \pm 1.4) \times 10^{-10}$ from the width difference $\Gamma(\rho^0 \to \pi^+\pi^-\gamma) - \Gamma(\rho^+ \to \pi^+\pi^0\gamma) = (0.45 \pm 0.45)$ MeV [30].

Summing all these corrections, the overall isospin-violating correction and its uncertainty are estimated to be $(-13.7 \pm 2.5) \times 10^{-10}$. These corrections relate the $\tau$ spectral function to the "pure" $e^+e^- \to \pi^+\pi^-$ with all QED corrections switched off. Since the $\sigma_{\rm had}^0$ term in Eq.(19) must include processes with the final state radiation (FSR) photons coming from the process $e^+e^- \to V\gamma \to \pi^+\pi^-\gamma$, we must reintroduce the FSR contributions [5]. After including those contributions $(+4.2 \times 10^{-10})$ [5], the total correction becomes $(-9.5 \pm 2.5) \times 10^{-10}$.

With the external parameters in Table X and corrections discussed above, we obtain $a_\mu^{\pi\pi}$ over the range $\sqrt{s} = 2m_\pi - 1.80$ GeV/$c^2$

$$a_\mu^{\pi\pi}[2m_\pi, 1.80\ {\rm GeV}/c^2] = (523.5 \pm 1.1\,({\rm stat.}) \pm 1.0\,({\rm sys.}) \pm 2.6\,({\rm Br.}) \pm 2.5\,({\rm isospin})) \times 10^{-10},$$

where the first error is statistical, the second is the experimental systematic (Table XI), the third comes from the uncertainties on the branching fractions (Table X), and the fourth is from isospin-violating corrections (Table XII).


[1] Throughout this paper, the inclusion of the charge-conjugate decay mode is implied unless stated otherwise.

[2] M. Davier and W.J. Marciano, Ann. Rev. Nucl. Part. Sci. **54**, 115 (2004).

[3] M. Passera, J. Phys. G **31**, R75 (2005).

[4] F. Jegerlehner, Acta Phys. Polon. B **38**, 3021 (2007).

[5] M. Davier, S. Eidelman, A. Höcker and Z. Zhang, Eur. Phys. J. C **27**, 497 (2003).

[6] M. Davier, S. Eidelman, A. Höcker and Z. Zhang, Eur. Phys. J. C **31**, 503 (2003).

[7] K. Hagiwara, A.D. Martin, D. Nomura, and T. Teubner, Phys. Lett. B **557**, 69 (2003).
[8] M. Davier, A. Höcker and Z. Zhang, Rev. Mod. Phys. **78**, 1043 (2006).
[9] M. Davier and A. Höcker, Phys. Lett. B **435**, 427 (1998).
[10] R. R. Akhmetshin *et al.* (CMD-2 Collaboration), Phys. Lett. B **527**, 161 (2002).
[11] R. R. Akhmetshin *et al.* (CMD-2 Collaboration), Phys. Lett. B **578**, 285 (2004).
[12] V. M. Aulchenko *et al.* (CMD-2 Collaboration), JETP Lett. **82**, 743 (2005).
[13] V. M. Aulchenko *et al.* (CMD-2 Collaboration), JETP Lett. **84**, 413 (2006).
[14] R. R. Akhmetshin *et al.* (CMD-2 Collaboration), Phys. Lett. B **648**, 28 (2007).
[15] A. Aloisio *et al.* (KLOE Collaboration), Phys. Lett. B **606**, 12 (2005).
[16] M.N. Achasov *et al.* (SND Collaboration), JETP **101**, 1053 (2005).
[17] M.N. Achasov *et al.* (SND Collaboration), JETP **103**, 380 (2006).
[18] R. Barate *et al.* (ALEPH Collaboration), Z. Phys. C **76**, 15 (1997).
[19] S. Schael *et al.* (ALEPH Collaboration), Phys. Rep. **421**, 191 (2005).
[20] S. Anderson *et al.* (CLEO Collaboration), Phys. Rev. D **61**, 112002 (2000).
[21] M. Artuso *et al.* (CLEO Collaboration), Phys. Rev. Lett. **72**, 3762 (1994).
[22] K. Ackerstaff *et al.* (OPAL Collaboration), Eur. Phys. J. C **7**, 571 (1999).
[23] K. Ackerstaff *et al.* (OPAL Collaboration), Eur. Phys. J. C **4**, 193 (1998).
[24] M. Acciarri *et al.* (L3 Collaboration), Phys. Lett. B **345**, 93 (1995).
[25] J. Abdallah *et al.* (DELPHI Collaboration), Eur. Phys. J. C **46**, 1 (2006).
[26] S. Eidelman, Talk at XXXIII Int. Conf. on High Energy Phys., Moscow, 2006, Acta. Phys. Polon. B **38**, 3015 (2007).
[27] M. Davier, Nucl. Phys. Proc. Suppl. **169**, 288 (2007).
[28] G.W. Bennett *et al.* (Muon g-2 Collaboration), Phys. Rev. D **73**, 072003 (2006).
[29] K. Hagiwara, A.D. Martin, D. Nomura, and T. Teubner, Phys. Lett. B **649**, 173 (2007).
[30] V. Cirigliano, G. Ecker and H. Neufeld, Phys. Lett. B **513**, 361 (2001). V. Cirigliano, G. Ecker and H. Neufeld, J. High Energy Phys. **08**, 002 (2002).
[31] W.-M. Yao *et al.* (PDG2006), J. Phys. G: Nucl. Part. Phys. **33**, 1 (2006) and 2007 partial update for edition 2008.
[32] N. Cabibbo, Phys. Rev. Lett. **10**, 531 (1963); M. Kobayashi and T. Maskawa, Prog. Theor. Phys. **49**, 652 (1973).
[33] The definition of the weak spectral function (or form factor) used in this paper ($v_-(s)$) differs by a factor of $\sqrt{2}$ from the one ($v_-^w(s)$) used in the other literature: $v_-(s)^w = \sqrt{2}v_-(s) = \sqrt{2}v_0^{I=1}(s)$. See, for example, A.Z. Dubničkova, S. Dubnička and M.P. Rekalo, Czechoslovak, Jour. Phys., **43**, 1057 (1993).
[34] The formula for $\beta_-(s)$ is an approximate one where the term proportional to $m_{\pi^-}^2 - m_{\pi^0}^2$ is ignored. In this approximation, the $\pi^-$ and $\pi^0$ energies in the $(\pi^-\pi^0)$ rest-frame are given by $E_{\pi^-}^* = E_{\pi^0}^* = \sqrt{s}/2$.
[35] S. Kurokawa and E. Kikutani, Nucl. Instr. and Meth. A **499**, 1 (2003) and other papers included in this Volume.
[36] A. Abashian *et al.* (Belle Collaboration), Nucl. Instr. and Meth. A **479**, 117 (2002).
[37] S. Jadach, B.F.L. Ward, Z. Wąs, Comp. Phys. Commun. **130**, 260 (2000); Phys. Rev. **D63**, 113009 (2001).
[38] S. Jadach and Z. Wąs, Comp. Phys. Commun. **85**, 453 (1995); ibid., **64**, 267 (1991); ibid., **36**,191 (1985); S. Jadach, J.H. Kühn, and Z. Wąs, Comp. Phys. Commun. **64**, 275 (1991); ibid., **70**, 305 (1992); ibid., **76**, 361 (1993).
[39] Z. Wąs and P. Golonka, Nucl. Phys. Proc. Suppl. **144**, 88 (2005).

[40] S. Eidelman *et al.*, Phys. Lett. B **592**, 1 (2004).
[41] S. Banerjee, B. Pietrzyk, J. M. Roney, Z. Wąs, Phys. Rev. D **77**, 054012 (2008).
[42] P. Golonka, B. Kersevan, T. Pierzchala, E. Richter-Wąs, Z. Wąs and M. Worek, Comput. Phys. Commun. **174**, 818 (2006).
[43] The QQ $B$ meson decay event generator was developed by the CLEO Collaboration. See http://www.lns.cornell.edu/public/CLEO/soft/QQ.
[44] S. Jadach *et al.*, Comp. Phys. Commun. **102**, 229 (1997).
[45] F.A. Berends, P.H. Daverveldt, and R. Kleiss, Comp. Phys. Commun. **40**, 285 (1986).
[46] R. Brun *et al.*, GEANT 3.21, CERN Report No. DD/EE/84-1 (1987).
[47] A. Lopez *et al.* (CLEO Collaboration), Phys. Rev. Lett. **99**, 122001 (2007).
[48] B. Aubert *et al.* (BaBar Collaboration), Phys. Rev. D **76**, 051104 (2007).
[49] A. Höcker and V. Kartvelishvili, Nucl. Instr. Meth. A **372**, 469 (1996).
[50] G.J. Gounaris and J.J. Sakurai, Phys. Rev. Lett. **21**, 244 (1968).
[51] See Eq.(32.11), p 302 in Ref. [31]. For the cases when the difference in the number of degrees of freedom is greater than one, the significance can be evaluated by the routine GAUSIN in the CERN library.
[52] M. Benayoun *et al.*, Eur. Phys. J., C **55**, 199 (2008). In this paper, the authors consider all decays of the $\rho$, $\omega$ and $\phi$ mesons consistently taking into account their mixings and provide good description of the pion form factor from $\tau$ lepton data below 1 GeV.
[53] F. Flores-Baéz, A. Flores-Tlalpa, G. López Castro and G. Toledo Sánchez, Phys. Rev. D **74**, 071301(R) (2006); A. Flores-Tlalpa, F. Flores-Baéz,G. López Castro and G. Toledo Sánchez, Nucl. Phys. Proc. Suppl. **169**, 250 (2007).
[54] W. J. Marciano and A. Sirlin, Phys. Rev. Lett. **61**, 1815 (1988).
[55] E. Braaten and C. S. Li, Phys. Rev. D **42**, 3888 (1990).
[56] J. Erler, Rev. Mex. Fis. **50**, 200 (2004).